Atmos. Chem. Phys. Discuss., 13, 11537–11595, 2013
www.atmos-chem-phys-discuss.net/13/11537/2013/
doi:10.5194/acpd-13-11537-2013

Atmospheric Chemistry and Physics Discussions
Open Access

A global climatology of stratosphere-troposphere exchange using the ERA-interim dataset from 1979 to 2011

B. Skerlak, M. Sprenger, and H. Wernli

ETH Zurich, IAC, Universitätstrasse 16, 8092 Zürich, Switzerland

Received: 15 March 2013 – Accepted: 23 March 2013 – Published: 2 May 2013

Correspondence to: B. Skerlak (bojan.skerlak@env.ethz.ch)

Published by Copernicus Publications on behalf of the European Geosciences Union.

Abstract

In this study we use the ERA-Interim reanalysis dataset from the European Centre for Medium-Range Weather Forecasts (ECMWF) and a refined version of a previously developed Lagrangian methodology to compile a global 33 year climatology of stratosphere-troposphere exchange (STE) from 1979 to 2011. Fluxes of mass and ozone are calculated across the tropopause, pressure surfaces in the troposphere, and the top of the planetary boundary layer (PBL). This climatology provides a state-of-the-art quantification of the geographical distribution of STE and the preferred transport pathways, and insight into the temporal evolution of STE during the last 33 yr.

We confirm the distinct zonal and seasonal asymmetry found in previous studies using comparable methods. The subset of "deep STE", where stratospheric air reaches the PBL within 4 days or vice versa, shows especially strong geographical and seasonal variations. The global hotspots for deep STE are found along the west coast of North America and over the Tibetan Plateau, especially in boreal winter and spring. An analysis of the time series reveals significant positive trends of the net downward mass flux and of deep STE in both directions.

The downward ozone flux across the tropopause is dominated by the seasonal cycle of ozone concentrations at the tropopause and peaks in summer, when the mass flux is nearly at its minimum. For the subset of deep STE events, the situation is reversed and the downward ozone flux into the PBL is dominated by the mass flux and peaks in early spring. Thus surface ozone concentration along the west coast of North America and around the Tibetan Plateau are likely to be influenced by deep stratospheric intrusions.

Quantitatively, all our results depend on the minimum residence time τ used to filter out transient STE trajectories. This dependence is shown to be a power law with exponents ranging between −0.44 and −0.87 for mass and ozone fluxes in both directions.

ACPD
13, 11537–11595, 2013

1 Introduction

Stratosphere-troposphere exchange (STE) has an important impact on atmospheric chemistry: it changes the oxidative capacity of the troposphere (e.g. Kentarchos and Roelofs, 2003) and potentially also affects the climate system because ozone and water vapour are potent greenhouse gases (e.g. Gauss et al., 2003; Forster et al., 2007). Although most ozone in the troposphere is produced photochemically (e.g. Jacobson, 2002), stratospheric ozone can be brought into the troposphere during STE events as found about 50 yr ago (Junge, 1962; Danielsen, 1968).

Modelling studies (e.g. Roelofs and Lelieveld, 1997) indicate that the stratospheric contribution to ozone in the troposphere could be as large as that from net photochemical production, which was also confirmed in a more recent multi-model ensemble simulation (Stevenson et al., 2006). This contribution, albeit only known with rather large uncertainty (Wild, 2007), is likely to increase over the next decades (Zeng and Pyle, 2003; Collins et al., 2003; Hegglin and Shepherd, 2009), which further emphasizes the importance of STE for tropospheric chemistry.

While ozone in the upper troposphere is mainly relevant as a greenhouse gas and oxidiser, deep STE down to the surface can also contribute to enhanced ozone levels at the ground and affect plant and human physiology (e.g. Lippmann, 1989; Knowlton et al., 2004). It is therefore not only important to quantify the global net ozone flux across the tropopause but also to investigate the transport and mixing after the crossing (e.g. Bourqui and Trepanier, 2010). The question of where and how often stratospheric intrusions can reach the planetary boundary layer and to what percentage STE contributes to total ozone levels at the ground is a topic of ongoing research (e.g. Davies and Schuepbach, 1994; Stohl et al., 2000; Vingarzan, 2004; Cooper et al., 2005; Trickl et al., 2010; Cristofanelli et al., 2010; Lefohn et al., 2011, 2012; Kuang et al., 2012).

The current study provides a global climatology of STE from 1979 to 2011 based on a refined version of the Lagrangian method introduced by Wernli and Bourqui (2002) (hereafter abbreviated as WB02) and the state-of-the-art reanalysis dataset

ACPD
13, 11537–11595, 2013

ERA-Interim from the ECMWF. This methodology allows to study the transport pathways from the stratosphere to the troposphere (STT) and from the troposphere to the stratosphere (TST). Of particular interest are so-called "deep" exchange events where stratospheric air, which typically is rich in ozone, reaches the planetary boundary layer (PBL) (deep STT) or potentially polluted air from the PBL is rapidly transported into the stratosphere (deep TST).

Climatologies using meteorological data, with a spatial and temporal resolution high enough to capture important synoptic systems (e.g. Sprenger and Wernli, 2003; James et al., 2003a, hereafter abbreviated as SW03 and JA03, respectively) nicely complement global-scale estimates (e.g. Holton et al., 1995) and synoptic-scale modelling case studies (e.g. Lamarque and Hess, 1994; Bourqui, 2006). The Lagrangian method used in this study also has several advantages over other methods such as the budget approach (Appenzeller et al., 1996), which does not allow for a study of the transport pathways, the Eulerian Wei method (Wei, 1987), which additionally suffers from errors due to the cancellation of large terms (Wirth and Egger, 1999) and large sensitivity to errors in the input fields (Gettelman and Sobel, 2000), and isentropic trajectory calculations (Seo and Bowman, 2001), which are frequently limited to a few isentropes and thus miss a significant amount of exchange events (SW03). A good overview of previous climatologies of STE, the methods used and their limitations is given in the review paper of Stohl et al. (2003) and the studies of Wirth and Egger (1999) and WB02.

This paper is structured as follows: we first describe the dataset and the refinements of the methodology in Sect. 2. Then we present the climatology of the cross-tropopause mass flux in Sect. 3, followed by the results for the cross-tropopause ozone flux in Sect. 4. In Sect. 5, we discuss aspects of the methodology, compare our results to the findings of SW03 and other studies, and elaborate some regional aspects. Finally, we present our conclusions in Sect. 6.

ACPD
13, 11537–11595, 2013

2 Data and methodology

2.1 Overview

The reanalysis dataset ERA-Interim from the ECMWF (Simmons et al., 2006; Dee et al., 2011) is continuously updated and covers the time from 1 January 1979 to the present day. Our analysis covers the first 33 yr from 1979 up to and including 2011. The primary analysis fields (e.g. wind and temperature) were interpolated on a regular grid with 1° horizontal resolution and the secondary fields like potential temperature (Θ) and potential vorticity (PV) (Ertel, 1942) were then calculated on the original hybrid model levels as described in SW03. The Lagrangian methodology presented in WB02 and applied to the ERA-15 dataset in SW03 was further developed and used to calculate mass and ozone fluxes across the tropopause, pressure surfaces in the middle and lower troposphere (500, 600, 700 and 800 hPa) and the top of the PBL.

This methodology is based on a large set of trajectories started every 24 h on a regular grid spanning the whole globe between 650 hPa and 50 hPa. The spacing of this grid is approximately $\Delta x = 80$ km in the horizontal and $\Delta p = 30$ hPa in the vertical. In the tropics (between 30° S and 30° N) the vertical grid spacing is 10 hPa to accommodate for the typically slower vertical motion. Trajectories that cross the tropopause are extended for 4 days forward and backward, yielding trajectories with a total length of 9 days. The tropopause definition in our study is the common combination of the ±2 pvu isosurfaces and the 380 K isentrope (Hoskins et al., 1985; Holton et al., 1995). The crucial minimum residence time criterion (48 h) then removes transient exchanges and thus only "significant" exchange events are taken into account. Trajectories are kinematic, using the 3-dimensional wind fields from ERA-Interim, and calculated with the tool developed by Wernli and Davies (1997). See WB02 and SW03 for more details.

The two main enhancements of this methodology used in the current study are a more elaborated distinction between the troposphere and the stratosphere using a 3-D-labelling algorithm and an altered definition of vertically deep exchange events, which is more relevant for understanding surface ozone concentrations.

ACPD
13, 11537–11595, 2013

2.2 3-D-labelling

Outside the tropics, an STE event can in principle be detected as a transition of the trajectory's PV from below to above 2 pvu (−2 pvu in the Southern Hemisphere) or vice versa. However, there are diabatically produced PV structures in the troposphere and low-level PV anomalies due to friction, for instance near mountains. If their PV value exceeds 2 pvu, they can be mistaken as stratospheric air. We have therefore used a refined version of the 3-D-labelling algorithm introduced in Sprenger et al. (2003) to separate tropospheric and stratospheric air more objectively. This algorithm not only combines the ±2 pvu and the 380 K criterion but also checks the connectivity of grid points with |PV| > 2 pvu to the stratosphere or the surface and assigns labels from 1 to 5 to every grid point, as illustrated in Fig. 1. STE events are thus identified as transitions from label 2 to 1 (STT) and 1 to 2 (TST) within 24 h.

Over Greenland and especially over Antarctica, very stable air masses just above the surface often have high PV values and are thus given the label 5. If such a surface-bound PV anomaly comes in contact with a low tropopause, distinguishing between the anomaly and the stratosphere requires an additional criterion. Instead of the threshold in specific humidity chosen by Sprenger et al. (2003), which is problematic in the case of very dry air masses above Antarctica, our new criterion is of geometric nature. The label 2 can always propagate vertically and overrides label 5. As a consequence, the vertical column below an area of contact between label 2 and label 5 is given the label 2. The horizontal propagation of label 2 in such cases, however, is limited to the upper half of the troposphere (calculated for every column) which prevents the label 2 from being spread over a large area near the surface. The very few cases where a trajectory originating within a surface-bound PV anomaly (label 5) meets such a "stratospheric funnel" (label 2) and then enters the troposphere (label 1) are filtered out by demanding that the label remains constant for 48 h before and after the crossing.

ACPD
13, 11537–11595, 2013

2.3 Deep exchange events

The importance of vertically deep exchange events stems from the rapid exchange between the stratosphere and the PBL and their particular impact on atmospheric chemistry. In previous studies, deep exchange events were defined as trajectories with a maximum pressure greater than 700 hPa (WB02, SW03) or a minimum height smaller than 3 km (JA03). These are crude approximations to the PBL height, which ignore its diurnal cycle and geographical variation and limit the investigation to areas without high topography. Therefore, in this study, we use the PBL height from ERA-Interim 6-hourly forecasts to identify deep exchange events. A trajectory is thus only selected as a deep exchange if its pressure exceeds the pressure at the PBL top at any time step after the exchange (deep STT) or before the exchange (deep TST). The description of the scheme at ECMWF that determines the PBL height can be found in Dee et al. (2011) and references therein.

3 STE climatology: mass flux

Every trajectory represents $\Delta m \approx \frac{1}{g}(\Delta x)^2 \Delta p \approx 6.52 \times 10^{11}$ kg of air. The mass flux across a surface is thus calculated by counting the number of crossing trajectories and multiplying by Δm. The global mass fluxes in our study amount to $8.89 \times 10^{10}\,\mathrm{kg\,s^{-1}}$ (STT) and $8.75 \times 10^{10}\,\mathrm{kg\,s^{-1}}$ (TST) yielding a downward net flux of $1.33 \times 10^{9}\,\mathrm{kg\,s^{-1}}$, which is roughly two orders of magnitude smaller than the gross flux (STT + TST).

3.1 Geographical distribution

3.1.1 Total STT mass flux

The geographical distribution of the STT mass flux is shown in Fig. 2. In the Northern Hemisphere (NH), the storm tracks over the North Atlantic and North Pacific are the dominant regions for STT during all seasons (around $500\,\mathrm{kg\,km^{-2}\,s^{-1}}$, peak value in

ACPD
13, 11537–11595, 2013

DJF: 625 kg km^{-2} s^{-1}) except for JJA (around 350 kg km^{-2} s^{-1}). This agrees well with previous findings (e.g. SW03). The mountain chains in Asia such as the Himalayas (DJF, MAM), the Pamirs (DJF, MAM, JJA) and the Tian Shan (MAM, JJA) are also associated with intense STT flux (above 450 kg km^{-2} s^{-1}). The elevated STT flux over the North-Central US, Anatolia and the northern side of the Tibetan Plateau in JJA are likely due to intense tropopause folding activity (Sprenger et al., 2003).

In the Southern Hemisphere (SH), two zonal bands around 35° S and 65° S show an enhanced STT mass flux. The band along the subtropical jet (STJ), where tropopause folds occur preferentially, is clearly visible in JJA with peaks over the east and west coasts of Australia and the Northern Tasman Sea (around 425 kg km^{-2} s^{-1}). In SON and DJF, the main peak is located over the Andes (reaching 500 kg km^{-2} s^{-1}), and the southern tip of Africa shows elevated values (up to 350 kg km^{-2} s^{-1}) in all seasons. STT along the storm track over the Southern Ocean is quite uniform in SON and DJF and becomes more localized over Wilkes Land in East Antarctica during MAM and JJA (up to 450 kg km^{-2} s^{-1}). A possible explanation for this is the combination of high orography and a tropopause that is typically lower than the zonal mean (especially in MAM).

3.1.2 Total TST mass flux

The annually averaged TST mass flux (Fig. 3) mainly shows large values poleward of approximately 55° latitude in both hemispheres and preferentially over the oceans and coastal regions. Distinct peaks are found along the north coast of Greenland (up to 475 kg km^{-2} s^{-1} in DJF and around 400 kg km^{-2} s^{-1} in MAM and SON) and along the coast of Antarctica, especially over Mac.Robertson land near 70° E (reaching 500 kg km^{-2} s^{-1} in MAM) and the transantarctic mountains around 165° E (peaking at 550 kg km^{-2} s^{-1} in MAM, around 475 kg km^{-2} s^{-1} in other seasons). As discussed above, the tropopause in these regions is typically lower than the zonal mean, facilitating the transport into the stratosphere.

ACPD
13, 11537–11595, 2013

In the subtropics, notable peaks are found over the eastern Mediterranean and Anatolia (up to 525 kg km^{-2} s^{-1} in JJA), the regions upstream of the continents around 30° S (all seasons), and over North Africa (JJA, SON, DJF). Tropopause folds are quite frequent in all these regions and are especially deep over Anatolia (Sprenger et al., 2003). The importance of the Western Pacific for tropical TST during the Asian monsoon period is well known (e.g. Fueglistaler et al., 2004; Gettelman et al., 2004). Indeed, enhanced TST is visible on the eastern flank of the upper-level anticyclone in Fig. 3 in JJA and to a lesser extent also in SON.

3.1.3 STT mass flux through pressure surfaces

As mentioned in the introduction, it is important to not only investigate the flux across the tropopause but also to follow the STT air parcels as they descend into the troposphere. This is of course also true for TST air parcels in the stratosphere, but due to the focus of this study on quantifying the stratospheric contribution to tropospheric ozone, we only discuss STT here. In Fig. 4, the mass flux across four pressure surfaces is depicted and the areas of highest flux across the tropopause are indicated with contours. Trajectories are only taken into account for these calculations after they crossed the tropopause. One clearly visible feature is the equatorward transport of the air parcels as they descend. The peaks in the flux across the 700 hPa surface are on average located 10–15° closer to the equator in the NH and approximately 20° in the SH than the peaks in the flux across the tropopause. This is readily explained by the sloping isentropes in the extratropics and a quasi-isentropic downward transport in the middle troposphere. The flux across the 700 hPa surface is dominated by exchanges in the North Atlantic and North Pacific storm tracks, a zonal band around 40° S originating from the storm track in the Southern Ocean and peaks over the South Central United States and Central Europe. What can also be seen from these plots is that only a small amount of exchange events is vertically deep and reaches a pressure of 700 hPa or more (roughly 10 %). Also, for obvious reasons, there is no flux below 700 hPa in areas with high orography such as the Himalayas. This illustrates the need for a refined

ACPD
13, 11537–11595, 2013

criterion for deep exchange events, compared to WB03, SW03 and JA03, that is also applicable in mountain areas.

3.1.4 Mass flux from deep STT events into the PBL

The especially interesting cases where stratospheric air reaches the PBL within a few days (deep STT) are shown in Fig. 5. The flux into the PBL is depicted in colors and the contours indicate where the flux across the tropopause is largest. Note that these contours do not directly correspond to the flux shown in Fig. 2 because only the subset of deep exchanges is taken into account here.

In both hemispheres, the subtropics around 30° and especially mountain ranges near those latitudes are the preferred regions of deep STT into the PBL. Very distinct maxima are found over the Rocky Mountains and the Northern Sierra Madre (up to 230 $kg\,km^{-2}\,s^{-1}$ in MAM), the Himalayas and the Tibetan Plateau (up to 215 $kg\,km^{-2}\,s^{-1}$ in DJF and to a lesser extent also in MAM and JJA). The maximum over the Himalayas and the Tibetan Plateau is explained by the combination of very high topography and a PBL that extends up to almost 3 km from the ground (Yang et al., 2004), which leads to PBL tops reaching pressures of 350 hPa and lower, allowing for a near-horizontal transport from the stratosphere into the PBL. The air masses transported to this region cross the tropopause over an area stretching from Northern Africa to the Pamirs. The peak over the Rockies is of different nature since both the topography and the PBL height are lower such that there is more vertical transport needed to reach the PBL. The air masses cross the tropopause at the end of the North Pacific storm track and slide down the isentropes in a south-eastward direction. This roughly corresponds to the situation shown by SW03 (their Fig. 6a).

The storm tracks in the North Atlantic and North Pacific are also areas of enhanced deep STT which is especially interesting because of the relatively shallow marine PBL. The entrance into the PBL is shifted approximately 20° equatorward from the crossing of the tropopause due to transport along sloping isentropes as discussed before. This implies that even areas south of 30° N can be affected by stratospheric air (Cooper

ACPD
13, 11537–11595, 2013

et al., 2005). Central Europe, North Africa and the Middle East are virtually only affected in DJF and MAM with the exception of some activity over Anatolia in JJA. We can confirm the finding of SW03 that a significant amount of air that enters the PBL over and near the Mediterranean crosses the tropopause over the European Alps (their Fig. 6c). In MAM and JJA, there is also some deep STT reaching the PBL around the Hindukush, the Pamirs, the Altay mountains, the Mongolian Plateau and Gobi desert.

In the SH, most deep STT occurs in the subtropics in JJA and SON with peaks over the Andes, the Karroo in South Africa and both over and upstream of Australia.

Note that Fig. 5 is to be compared with the "destinations" plot in SW03 (their Fig. 5a). An obvious example of how the 700 hPa criterion (used in SW03) and the PBL criterion (used here) for deep exchanges differ is the fact that the peak over the Tibetan Plateau in DJF is not visible in SW03.

3.1.5 Mass flux from deep TST events out of the PBL

The flux of air masses out of the PBL that will reach the stratosphere within 4 days (deep TST) is shown in Fig. 6. Clearly, the entrance of the North Atlantic and North Pacific storm tracks are preferred areas of deep TST in DJF (up to 125 $\mathrm{kg\,km^{-2}\,s^{-1}}$) and to a lesser extent in MAM and SON. The air masses then cross the tropopause roughly 20° poleward which agrees very well with the findings of SW03 in DJF (their Fig. 6d).

The Tibetan Plateau emerges as a distinct peak in DJF (275 $\mathrm{kg\,km^{-2}\,s^{-1}}$) and especially in MAM (380 $\mathrm{kg\,km^{-2}\,s^{-1}}$). A closer look at the data reveals that these air masses mainly cross the tropopause over the Northwestern Pacific (contour in Fig. 6), which corresponds to a fast upward and long-range eastward transport of approximately 6500 km in less than 4 days. In JJA, this eastward transport is slower and the air masses also cross the tropopause over East Siberia and the Northwestern Pacific around 50° N.

The Rocky Mountains and the adjacent areas to the east are regions of high deep TST flux out of the PBL during nearly the whole year with a maximum in MAM

ACPD
13, 11537–11595, 2013

($175\,kg\,km^{-2}\,s^{-1}$) and a minimum in DJF. Additional analysis reveals that in JJA and SON most of this air crosses the tropopause over the Hudson Bay, whereas in DJF and MAM this peak is shifted south over the Great Lakes area and the Canadian Shield (cf. contours in Fig. 6).

We only see a weak signal of deep TST mass flux out of the PBL over China's east coast in MAM and JJA and no signal over India and Indochina. This is interesting because several studies (e.g. Berthet et al., 2007; Chen et al., 2012) found intense deep TST activity in this area, which is strongly affected by anthropogenic emissions. A possible reason for this discrepancy is that Chen et al. (2012) used Flexpart (Stohl et al., 2005, with parameterised convective transport) and considered longer timescales. Our approach focuses on relatively fast (within 4 days) transport by the grid-scale winds, which is likely to underestimate deep convective transport over continents in summer. The different timescales used could also explain why the signal over North Africa and the Arabian Peninsula visible in Berthet et al. (2007), where 30 day backward trajectories were calculated, is not present in our study.

In the SH, the flux out of the PBL occurs predominantly between 20° S and 50° S. In SON and DJF, mainly the continents are affected, especially the region east of the Southern Andes (up to $110\,kg\,km^{-2}\,s^{-1}$) and the south coasts of Africa and Australia. In MAM and JJA, areas of intense deep TST fluxes are also found along the storm track over the Southern Ocean.

3.2 Zonally integrated fluxes

The meridional profiles of the zonally integrated values of STT, TST and net (STT-TST) mass fluxes are shown in Fig. 7. Also depicted are the fluxes due to deep exchange events across the tropopause (TP) and the top of the PBL. Overall, there is remarkably little interannual variability, indicating very robust patterns.

ACPD
13, 11537–11595, 2013

3.2.1 All exchanges

The STT mass flux features a broad peak in the extratropics in both hemispheres. The distribution in the NH is of triangular shape with a maximum around 45° N whereas the SH exhibits a double-peak structure caused by the superposition of two separate peaks near 30° S (due to the STJ) and near 60° S (due to the storm track over the Southern Ocean, cf. Fig. 2).

The TST mass flux shows a complex structure consisting of three peaks in both hemispheres: one around 55° N and 60° S due to the storm tracks (North Atlantic, North Pacific, Southern Oceans), one around 30° N and 30° S mainly due to the exchanges near the subtropical jet in the Mediterranean (NH) and upstream of the continents (NH and SH) (cf. Fig. 3). In addition, there are two tropical peaks around 10–15° in both hemispheres that are better visible in the seasonal averages and are smeared out by the meridional displacement of the Intertropical Convergence Zone (not shown).

The net mass flux is directed downward between 30° N and 70° N and between 25° S and 60° S and upward in the tropics between 25° S and 25° N, except for a narrow band with near-zero net fluxes right at the equator. Poleward of 70° N and 60° S, the net flux is very small and directed upward, which agrees well with earlier studies (Juckes, 1997; SW03, their Fig. 8).

3.2.2 Deep exchanges

Deep exchange trajectories cross the tropopause in the extratropics and low polar regions in both directions (STT and TST) and hemispheres (NH and SH). The distributions for deep STT and deep TST indeed look very similar. The deep TST peak is shifted about 5° to the north with respect to the peak of deep STT in the NH whereas in the SH the peaks are very well aligned. The peaks in the SH are located around 60° S whereas the ones in the NH are located a bit closer to the equator, around 50° N. The peaks of the mass flux into (STT) and out of (TST) the PBL are shifted, relative to the peaks of the TP crossings, towards the equator by roughly 15° in the NH and 20–30°

ACPD
13, 11537–11595, 2013

in the SH. This shift is qualitatively in line with the slope of the isentropes, which is particularly steep in the NH storm track regions. Note also that, in particular in the SH, the shift is larger for STT than TST, indicating that deep STT occurs on dry isentropes, whereas deep TST can be associated with saturated motion on moist isentropes from the PBL to the upper troposphere.

An interesting hemispheric difference is the greater intensity of deep STT and deep TST in the NH. The reason for this might be the more vigorous PBL dynamics over the more abundant NH continents.

3.3 Seasonal cycles

Monthly averages of STT and TST mass fluxes are calculated for the 33 yr covered in this climatology. As a simple measure of the seasonality within a year, we consider the quotient $S = \frac{\max - \min}{\max + \min}$ where max and min denote the maximum and minimum value of the averaged annual cycle, respectively. This measure is essentially the ratio of the amplitude of the cycle and its mean value such that $S = 1$ for a cycle with a minimum value of zero.

3.3.1 All exchanges

The seasonal cycle of the STT mass flux (Fig. 8a and b) has a pronounced sawtooth-like shape in the NH with a maximum in winter (DJF) when the cyclonic activity over the North Pacific and North Atlantic is greatest and a minimum around August and September. The minimum value is approximately 22 % smaller than the peak value and the seasonality as defined above is 12 %. In the SH (Fig. 8b), the seasonal cycle is more sinusoidal in shape and much weaker ($S = 3$ %) but its timing is roughly the same as in the NH with a peak in winter (July) and a minimum in summer (December and January).

The seasonal cycle of the TST mass flux in the NH (Fig. 8c) also shows a rather sinusoidal cycle with a maximum in November and a minimum in May ($S = 5$ %). In

ACPD
13, 11537–11595, 2013

the SH (Fig. 8d), a clear peak in March dominates the seasonal cycle. It is followed by a steep drop between April and June (due to less exchanges in the tropics) and a slow increase throughout the rest of the year (S = 9%).

Note that other than the NH and SH cycles of STT, which peak in the same season, the NH and SH cycles of TST have quite a different timing. In the NH, the maximum in TST is reached in late fall whereas in the SH, TST peaks in early fall, corresponding to a shift of two months. The minima on the other hand occur nearly at the same time, namely in May (NH, late spring) and June (SH, early winter).

In the NH, the STT and TST cycles are shifted by two to four months with TST occurring earlier in the year than STT. In the SH, the cycles of STT and TST are nearly reversed with the minimum of TST being close to the maximum of STT and vice versa. This asynchronous behaviour indicates that different meteorological phenomena contribute to the peaks in STT and TST, respectively.

The comparison of our seasonal cycles to previous studies is not straightforward because the authors used a different tropopause definition (Schoeberl, 2004), investigated only the extratropics (SW03; James et al., 2003b), or both (Olsen et al., 2004). Our results also do not fully agree with the classical study of Appenzeller et al. (1996) in which the net mass flux was found to have maxima in May (NH) and June (SH) and minima in September (NH) and October (SH). Our net mass flux (not shown) has broad maxima between January and March (NH) and June and August (SH) and minima in September (NH) and February (SH). The minimum in the NH and the maximum in the SH thus nicely agree and both our maximum in the NH and the minimum in the SH are, albeit not being the main peaks, clearly visible in Appenzeller et al. (1996). When we restrict our analysis to the extratropics, as done in SW03 and James et al. (2003b), we obtain a seasonal cycle whose timing agrees quite well with their results (not shown).

3.3.2 Deep exchanges

The seasonal cycle of the mass flux due to deep STT events is shown in Fig. 9. The cycle for deep STT is much more pronounced than the one for all exchanges and shows

ACPD
13, 11537–11595, 2013

a more sinusoidal shape. The maxima occur in winter and early spring (March in the NH and August in the SH) and the minima in summer (August in the NH and January in the SH). The minimum in summer in the NH is less than 10 % of the maximum value (S = 82 %) whereas in the SH the minimum reaches roughly 20 % of the peak value (S = 69 %). Our seasonal cycle of deep STT mass flux in the NH agrees very well with the results of SW03 and JA03.

The deep TST mass flux shows a less regular seasonal cycle in the NH: the flux is relatively constant from January to June followed by a sharp decrease with a minimum in August after which it steadily increases until January. In the SH, the deep TST mass flux shows a broad maximum between March and July and a minimum in December. The minimum is roughly 55 % of the maximum value in both hemispheres, which shows that the seasonal cycle of deep TST (S = 28 % in the NH and 29 % in the SH) is much less pronounced than the one of deep STT. The deep TST mass flux in the NH is quite sinusoidal in SW03 whereas we observe a steep drop in early summer. This difference is due to the intense mass flux out of the PBL over the Himalayas in spring (not shown), which is not captured by SW03.

3.4 Potential temperature distributions

3.4.1 All exchanges

The distributions of potential temperature (Θ) for all exchange events are depicted in Fig. 10. Due to the seasonal cycle of the isentropes, the exchanges in summer occur at higher values of Θ than in winter in both hemispheres and for both STT and TST. The Θ distributions for spring and fall are fairly similar, except for TST in the NH, where SON shows a much higher peak at Θ > 340 K than MAM. The reason for this is the intense TST mass flux in the subtropics over the West Indies and the Caribbean in this season (not shown). There is a clear relationship between Θ and the latitude at the exchange location. In the tropics, exchanges occur at high potential temperatures above 350 K and as the tropopause slopes down towards the polar regions, exchanges

ACPD
13, 11537–11595, 2013

in the extratropics occur at lower potential temperatures mainly between 280 K and 350 K.

All distributions show a clear main peak below 350 K, varying from 295 K (STT NH DJF) to 325 K (TST NH JJA). Additionally, a smaller peak between 330 K and 340 K is visible for STT in the SH especially in DJF, which is mainly due to exchanges over the Andes (see Fig. 2). The vast majority of exchange events above 350 K occur in the tropics and subtropics between 25° S and 30° N (STT) and between 35° S and 40° N (TST) (not shown).

As expected, TST is larger than STT at high Θ, which concurs with a net upward transport in the tropics (cf. Fig. 7). Both for STT and TST, a prominent peak occurs at 380 K due to our tropopause definition. However, less than 1 % (STT) and 3 % (TST) of all exchanges take place at 380 K. As expected, this peak is much stronger for TST than for STT and its geographical distribution is limited to a narrow band between 10° S and 10° N (not shown).

As already discussed in SW03, studies of STE that are limited to specific isentropes such as for example 330 K and 350 K (Seo and Bowman, 2001) capture only a fraction of all STE events and might produce a seasonal cycle that is not representative for total STE.

3.4.2 Deep exchanges

The Θ distributions for deep exchange events only are shown in Fig. 11. All peaks are sharper and limited to the region below 350 K, which is mainly due to the fact that very little deep exchange events occur in the tropics (cf. Fig. 7). A notable exception of the otherwise dominating single-peak structure is the deep STT distribution in the NH in JJA, which features a second, smaller peak around 330 K due to exchanges over the Eastern Mediterranean and Anatolia (not shown). Again, the summer peaks are found at higher Θ than the winter peaks. The seasonal variation of the most likely Θ is larger in the NH (20–25 K) than in the SH (10–15 K).

ACPD
13, 11537–11595, 2013

3.5 Time series

The time series over the 33 yr from 1979 to 2011 allows studying the temporal evolution of STE fluxes over a period that is longer than the previously longest climatologies of STE covering the 15 yr from 1979 to 1993 (SW03, JA03).

For both STT and TST mass fluxes shown in Fig. 12, there is no trend discernible from 1979 to 2000 (in agreement with the findings of SW03 for the ERA-15 period) after which both fluxes decline. The upward flux declines more strongly than the downward flux, resulting in a small increase in the net downward flux after 2000. Linear regression analysis for the whole time series yields significant (p value $\sim 10^{-7}$) trends for TST ($-1.11 \times 10^8\,\mathrm{kg\,s^{-1}\,yr^{-1}}$) and STT-TST ($0.89 \times 10^8\,\mathrm{kg\,s^{-1}\,yr^{-1}}$).

Since our study covers the whole globe, the non-zero global net downward mass flux has two possible interpretations: either the real net mass flux is zero and our result is within the numerical and methodological error or the mass of the troposphere is increasing. The latter case is accompanied by a rise in tropopause heights which was reported in many previous studies (e.g. Steinbrecht et al., 1998; Seidel and Randel, 2006; Schmidt et al., 2008). To further analyse this, we have calculated the average tropopause pressure, and an approximation to the mass of the troposphere, assuming hydrostatic balance, for every year from 1979 to 2011 (not shown). Linear regression analysis reveals highly significant ($p < 1.5 \times 10^{-4}$) trends of $-0.05 \pm 0.01\,\mathrm{hPa\,yr^{-1}}$ and $2.74 \times 10^{14}\,\mathrm{kg\,yr^{-1}}$, respectively, in agreement with the studies mentioned above. This calculation thus suggests that the non-zero net downward mass flux, albeit likely being over-estimated, is not a numerical artefact.

For deep exchanges, both the STT and the TST mass flux steadily increase over time. The trend obtained from linear regression analysis for the whole time series is about twice as strong and much more significant for the deep STT mass flux ($1.26 \times 10^7\,\mathrm{kg\,s^{-1}\,yr^{-1}}$, $p \approx 2 \times 10^{-4}$) than for the deep TST mass flux ($5.02 \times 10^6\,\mathrm{kg\,s^{-1}\,yr^{-1}}$, $p \approx 0.024$).

ACPD
13, 11537–11595, 2013

4 Ozone flux into the troposphere

The downward ozone flux is essentially the product of the number of trajectories crossing the tropopause (which is directly proportional to the mass flux) and the ozone mixing ratio at the location of the crossing. It is thus clear that areas of high STT mass flux also tend to show high downward ozone flux. Nevertheless, geographical and seasonal variations in ozone concentrations at the 2 pvu/380 K tropopause shown in Fig. 13 are large and have a strong impact on the ozone flux. The tropics show very high ozone mixing ratios (around 140 ppbv) in all seasons and minima below 60 ppbv can be found in the polar regions in winter. In the extratropics, there are especially high ozone concentrations at the tropopause in boreal spring and summer over the eastern US, the North Atlantic, the Middle East, and large parts of central Asia.

The total STT ozone flux calculated in our study amounts to 420 $\mathrm{Tg\,yr^{-1}}$ which is within the estimates from models ($556 \pm 154\ \mathrm{Tg\,yr^{-1}}$) (Stevenson et al., 2006) and observations ($550 \pm 140\ \mathrm{Tg\,yr^{-1}}$) (Solomon, 2007). All calculations with the ozone field of ERA-Interim of course crucially depend on its quality. Dragani (2011) found that overall the ozone field agrees well with independent observations and performs better than in the earlier ERA-40 reanalysis. The relative errors in total column ozone are within ±2 % between 50° S and 50° N but the vertical profiles show errors of up to 20 % in the lower stratosphere, which is the key region for our study. Therefore, our results on ozone fluxes have to be interpreted with these limitations in mind.

4.1 Geographical distribution

The geographical distribution of the STT ozone flux through the tropopause is shown in Fig. 14. Areas of intense STT mass flux such as the storm tracks in the North Atlantic, the North Pacific, and the Southern Ocean also tend to show elevated values of STT ozone flux. Nevertheless, there are some differences when comparing the mass flux (Fig. 2) with the ozone flux (Fig. 14) that originate from the strong seasonal and geographical variation of ozone at the tropopause (Fig. 13). In DJF, the

ACPD
13, 11537–11595, 2013

ozone concentrations over the NH storm tracks are rather small such that the dominant peak in ozone flux is located over the Andes in the SH (nearly 3000 $kg\,km^{-2}\,yr^{-1}$) where tropopause ozone concentrations are nearly twice as high. The peak over southern Greenland in the mass flux in MAM and SON is less prominent in the ozone flux due to the low ozone concentrations in this region. In JJA, the same areas show high mass and ozone fluxes (e.g. central North America, Anatolia, Pamirs, Tian Shan, North China, Korea). The JJA ozone flux is dominant in the NH whereas the mass flux is more balanced between the hemispheres, a consequence of the strong hemispheric contrast in ozone concentration at the tropopause. An additional peak in STT ozone flux is found along the equator over the Indian ocean (nearly 3000 $kg\,km^{-2}\,yr^{-1}$) due to the very high ozone concentrations at the tropical tropopause.

The global peaks of STT ozone flux are thus found over the Andes around 35° S in DJF, over the Himalayas and the southern side of the Tibetan Plateau in MAM (up to 3500 $kg\,km^{-2}\,yr^{-1}$), and over central North America, Anatolia, the Pamirs, Tian Shan as well as large parts of East Asia in JJA (also up to 3500 $kg\,km^{-2}\,yr^{-1}$). This finding is consistent with the studies of Hsu et al. (2005), who found a peak of STT ozone flux over the Tibetan Plateau in May, and of Tang et al. (2011).

The geographical distribution of the deep STT ozone flux into the PBL shown in Fig. 15 indicates the regions where surface ozone levels are most likely affected by stratospheric intrusions. Western North America (in MAM) and the Tibetan Plateau (in DJF, MAM and JJA) are the global hotspots with peaks values of more than 1000 $kg\,km^{-2}\,yr^{-1}$. For the calculation of this flux, the ozone concentration was kept constant within the troposphere, i.e. any loss due to chemical processes and mixing was neglected and therefore, these values provide an upper boundary estimate. Nevertheless, our findings are in agreement with observational studies in these areas, which find a significant stratospheric influence (e.g. Cristofanelli et al., 2010; Lefohn et al., 2011, 2012).

ACPD
13, 11537–11595, 2013

4.2 Seasonal cycle

The seasonal cycle of the STT ozone flux (top row in Fig. 16, $S = 25\,\%$ in the NH and $S = 13\,\%$ in the SH) shows a very different pattern than the STT mass flux (top row in Fig. 8). Indeed, maxima of the ozone flux occur when the mass flux is nearly at its minimum and vice versa. The explanation for this result is that the ozone concentration at the tropopause during STT events (bottom row in Fig. 16) shows a nearly sinusoidal seasonal cycle with a maximum in summer (around 130 ppbv in the NH and 105 ppbv in the SH) and a minimum in winter (around 75 ppbv in the NH and 80 ppbv in the SH). Even though the mass flux in summer is about 20 % smaller than in winter, the ozone concentration is around 65 % larger and thus overcompensates the reduction in mass flux. This can also be quantified in terms of the seasonality S: for the STT mass flux, $S = 12\,\%$ in the NH and $S = 3\,\%$ in the SH (cf. Sect. 3.3), whereas the ozone concentrations at the tropopause have a larger seasonality, namely $S = 28\,\%$ in the NH and $S = 14\,\%$ in the SH.

In contrast to the total ozone flux, the ozone flux for deep exchange events only (middle row in Fig. 16) largely agrees in its timing with the mass flux (top row in Fig. 9). This is because the seasonality of the mass flux is large enough to dominate the ozone flux: its value in summer is reduced by approximately 90 % compared to winter ($S = 82\,\%$ in the NH and $S = 69\,\%$ in the SH, cf. Sect. 3.3). The peak in deep STT ozone flux is slightly shifted (one month later compared to the mass flux) in both hemispheres. This is due to the increase of ozone concentrations at the tropopause during the first half of the year in the NH and the second half of the year in the SH (cf. bottom row in Fig. 16). A remarkable feature is that while the seasonal cycle of deep STT is similar to the whole STT mass flux, this is not true for the ozone flux. In fact, the deep STT ozone flux is shifted by roughly 4 months with respect to the STT ozone flux and peaks in early spring.

ACPD
13, 11537–11595, 2013

4.3 Time series

The global STT ozone flux shown in Fig. 17 slightly increases from 1979 to late 1991. It then is reduced during three years and increased notably between 1994 and late 2001. Between early 2002 and mid 2003, there is a striking jump and the ozone flux is roughly halved. Afterwards, it recovers again in 2004, stays nearly constant for four years and begins to slightly decrease after 2009. Details on these spurious jumps and possible explanations are discussed in Sect. 5.1.

4.4 Ozone flux through pressure surfaces and dependence on minimum residence time

The ozone flux through pressure surfaces can be calculated analogously to the mass flux (Sect. 3.1.3). Only trajectories that already have crossed the tropopause (STT) are taken into account and as for the calculation of the deep STT ozone flux, the ozone concentration along a trajectory is kept constant after crossing the tropopause. Since our results depend strongly on the minimum residence time it is worthwile to examine this dependency in more detail. Clearly, the total STT ozone flux is smaller across pressure surfaces in the lower troposphere than across the tropopause and also, a decrease of the flux with increasing minimum residence time τ is expected. The results depicted in Fig. 18 show that this is indeed the case and that the dependency on τ is, to very good approximation, a power law ($c \cdot \tau^{\kappa}$ with some constant c). The fitted exponents κ for the ozone flux across the pressure surfaces below 500 hPa and into the PBL are close to -0.5 (-0.46 ± 0.01) and for the 400 hPa surface and the tropopause, the fitted exponents are -0.56 ± 0.01 and -0.77 ± 0.02, respectively. The power law applies with remarkable precision: all coefficients of determination, R^2, are greater than 0.995. These results are in agreement with theory, which suggests that for any advective-diffusive flow, the (mass) flux across a control surface such as the tropopause is proportional to $\tau^{-0.5}$ for small τ in the continuum limit (Hall and Holzer, 2003; Orbe et al., 2012). Note though that the τ used in these studies is only a one-sided criterion, i.e. it is only

ACPD
13, 11537–11595, 2013

required that the air parcel stays for at least τ in the stratosphere (in the case of STT), whereas our minimal residence time τ is required both before and after the exchange.

5 Discussion

In this section, we want to address caveats of the method, compare our results to previous studies and discuss our results in selected regions.

5.1 Caveats of the method

The quantitative results in this study depend on the choice of the minimum residence time τ. This is a fundamental property of any advective-diffusive flow across a control surface such as the tropopause (Hall and Holzer, 2003; Orbe et al., 2012). We find that both the mass flux (not shown) and the ozone flux (Fig. 18) scale as τ^{κ} with an exponent κ depending on the height of the control surface. At the tropopause, $\kappa \approx -0.75$, and for pressure surfaces in the troposphere and the PBL, $\kappa \approx -0.5$ (see Sect. 4.4). The fitted exponents for the mass flux below 500 hPa are even closer to -0.5 (-0.49 ± 0.01), and at the tropopause and the 400 hPa surface, the fitted exponents are -0.76 and -0.58, respectively. The power law applies with very good precision and for fairly large τ up to 96 h, indicating that our calculated STE flux, at least for the lower pressure surfaces and the PBL, is clearly in the diffusive regime described in Hall and Holzer (2003). The geographical patterns of the flux, on the other hand, are not very sensitive to this parameter (not shown) such that our choice of 48 h (see Sect. 2) mainly affects the amplitude of the flux. A thorough discussion on the sensitivity of the methodology to the parameter τ can be found in Bourqui (2001), WB02 and Bourqui (2006).

Our methodology to quantify deep STE relies strongly on the quality of the diagnosed PBL height in the ECMWF model. An entraining parcel method is used to select the top of stratocumulus or the cloud base in shallow convection situations (Dee et al., 2011). The obtained values seem meaningful in most areas but over the Tibetan Plateau, with

ACPD
13, 11537–11595, 2013

values of 300 hPa and less, the PBL height is likely overestimated. Measurements show that it can extend to almost 3000 m above ground (Yang et al., 2004) which together with terrain heights of 5000 m a.s.l. can lead to pressures of about 330 hPa at the top of the PBL. We thus discarded all deep STE events where the PBL top reached higher than this value. This restriction changes the amplitude of the peak over the Tibetan Plateau for both deep STT and deep TST. Compared to no limit applied, the peak as it is shown in Figs. 5 and 6 is reduced by a factor of approximately two. The very high-reaching PBL thus clearly plays an important role for quantifying deep STE in this region.

Although the ozone field in ERA-Interim agrees reasonably well with independent measurements, there are uncertainties on the order of 10 % (Dragani, 2011) and spurious jumps occur in the time series (Fig. 17). Ozone values in the years between 1995 and 2004 could suffer from changes in the assimilated satellite data, as described in Dragani (2011). In 1995, ozone data from only one satellite instrument (NOAA-9 SBUV) was assimilated in ERA-Interim, and during 1996 and 1997, 4 new instruments were added. In the following 5 yr, the STT ozone flux increases strongly before dropping by nearly 50 % in 2002 and 2003, which is likely due to 3 instruments going out of service and being replaced by 3 new satellite instruments. An in-depth investigation of the assimilation procedure in these years would be necessary to fully unravel this puzzling behaviour, which clearly prevents us from performing a trend analysis of the STT ozone flux.

A drawback of any Lagrangian method relying on trajectories calculated from resolved wind fields is the underestimation of convective fluxes due to sub-grid scale processes. Tang et al. (2011) have found that deep convection reaching into the stratosphere mainly contributes to the STE ozone flux over the continents in NH spring and summer and enhances it by 19 %. Over the oceans, during the rest of the year and in the SH, the contribution is much smaller.

ACPD
13, 11537–11595, 2013

5.2 STE mass flux: comparison to SW03 and other studies

Compared to the earlier reanalysis dataset ERA-15 used by SW03 and JA03, the increased spatial resolution of ERA-Interim (T255 in the horizontal and 60 levels up to 0.1 hPa in the vertical), the 4-D-Var data assimilation scheme and the strongly increased assimilation of satellite observations constitute major advances leading to an increased overall quality. Especially areas with sparse data such as the tropopause region are represented smoother and more realistically (Dee et al., 2011). Also, the current climatology is compiled globally instead of only for the NH extratropics in SW03 and covers a longer period (33 yr vs. 15 yr). The methodology is refined in mainly two points: A 3-D-labelling algorithm is used to distinguish between stratospheric air and isolated PV anomalies in the troposphere and a new definition of deep exchange using the PBL height is introduced and replaces the 700 hPa surface used in SW03.

Our results for the STT mass flux in the NH shown in Fig. 2 generally confirm the findings of SW03 (their Figs. 2 and 4): the North Atlantic and North Pacific storm tracks are the regions with the largest STT mass flux. In the current study, the peak over the North Pacific is much more confined to the ocean than in SW03. This is probably due to a data assimilation problem in ERA-15, where radiosonde data clearly dominated the assimilation at the tropopause level and led to pronounced assimilation increments over the continents. In ERA-Interim, the assimilation increments are much smoother due to the large number of assimilated satellite data. Note that due to the different minimum residence time values, 48 h here and 96 h in SW03, the quantitative values of all mass fluxes are larger by a factor of about two.

The TST mass flux resembles very much the one of SW03 in the regions north of 20° N. In JJA, we report a strong peak over the Eastern Mediterranean and Anatolia, which was present yet less pronounced in SW03.

The potential temperature distribution of all STT events in the NH is similar to the results in SW03 (their Fig. 3), although the new distributions are broader due to exchanges in the tropics not included in SW03. The first peak at roughly 320 K in JJA

ACPD
13, 11537–11595, 2013

is clearly smaller than the one for the winter period (DJF) at 296 K, which was not the case in SW03.

The mass flux of deep STT events into the PBL (top left in Fig. 5) and deep TST out of the PBL (top left in Fig. 6) in DJF can in principle be compared to the "destinations" (STT) and "origins" (TST) of SW03 (their Fig. 5), yet the different criteria for deep events clearly have a large impact. For deep STT, the end of the North Pacific storm track, the southern and eastern US, and the start of the North Atlantic storm track are the preferred "destinations" in SW03. In our study, these areas also show high STT fluxes into the PBL, but the peak over the west coast of North America is shifted inland and the peak in the eastern US is shifted over the Atlantic. Furthermore, SW03, by definition of their criterion for deep STE, could not investigate trajectories that enter the PBL above high altitude orography such as the Tibetan Plateau, which proves to be of high importance in this study. The situation for deep TST is similar because both studies emphasize the role of the starting regions of both NH storm tracks but the peaks over the Tibetan Plateau and the mountain chains in western North America were not visible in SW03.

In order to compare our results for the total mass flux to previous studies, it is necessary to look at the tropopause in the extratropical NH only (here defined as the region north of 30° N). Although our STT and TST fluxes across the extratropical tropopause ($110.2 \times 10^{16}\,\mathrm{kg\,yr^{-1}}$ and $91.0 \times 10^{16}\,\mathrm{kg\,yr^{-1}}$, respectively) are about 40 times smaller than the values in JA03, the net flux of $19.2 \times 10^{16}\,\mathrm{kg\,yr^{-1}}$ is of the same order of magnitude ($44.0 \times 10^{16}\,\mathrm{kg\,yr^{-1}}$ in JA03) and lies at the lower end of the range of values listed in Olsen et al. (2004, their Table 1).

We also computed the fluxes for an alternative tropopause definition using 3.5 pvu and 380 K (whichever is lower). The STT flux is reduced by about 40 % when compared to the 2 pvu definition but the main patterns of the geographical distributions are robust (not shown). The same is true for the TST flux which is reduced by roughly 30 %. The number of deep exchanges is strongly reduced, as expected. For deep STT, the main peak is over the North Pacific storm track (~70 % less) and for deep TST, the values

ACPD
13, 11537–11595, 2013

over this storm track and in the area from the Hudson Bay to Iceland are reduced by ∼ 80 %.

5.3 STT Ozone flux: comparison to other studies

A first way to compare our results to other studies is to look at the mean ozone mixing ratio at the tropopause shown in Figs. 13 and 16 (bottom row). We find a nearly sinusoidal seasonal cycle with a maximum in summer and a minimum in winter and a fairly large interannual variability. Our seasonal cycle agrees well with measurements from the MOZAIC campaign (Marenco et al., 1998) over the North Atlantic and Europe. Thouret et al. (2006) found a sinusoidal cycle of ozone at the 2 pvu tropopause with a maximum in May (120 ppbv) and a minimum in November (65 ppbv). If we restrict our analysis to exchanges occurring in the same region, we find a peak in June (120 ppbv) and a minimum in December (70 ppbv). Our cycle is thus shifted in time by one month with respect to the MOZAIC measurements and agrees very well in amplitude.

A more in-depth comparison to other studies is necessary for the seasonal cycle of the STT ozone flux shown in Fig. 16 because it not only depends on the ozone mixing ratio at the tropopause but also on the STT mass flux. The situation is quite complicated though because, as Hsu et al. (2005) wrote, "there appears to be no agreement as to when and where stratospheric O_3 enters the troposphere". Part of this uncertainty is due to different choices of definitions for the tropopause and the extratropics. In the studies using chemistry transport models (CTM) and refined versions of the methodology by Appenzeller et al. (1996), the tropopause is defined as 2 pvu (Hegglin and Shepherd, 2009), 3.5 pvu (Olsen et al., 2004), ozone mixing ratio of 100 ppbv (Hsu et al., 2005) or even 95 hPa in the tropics and 256 hPa in the extratropics (Gettelman et al., 2004). Nevertheless, all these studies roughly agree in the timing of the STT ozone flux maximum (NH: between March and June, SH: in SON) and minima (NH: SON, SH: JFM). The amplitudes of the flux vary considerably for the NH minimum (between 3.9 and 20 Tg month^{-1}) but agree within a factor of two for the NH maximum (33–45 Tg month^{-1}) and both the SH maximum (27–50 Tg month^{-1}) and minimum (13–

ACPD
13, 11537–11595, 2013

20 Tg month^{-1}). Note that even though the method used in these studies only yields the net mass flux, Olsen et al. (2004) subdivided the ozone field in a stratospheric and tropospheric part, allowing for the calculation of STT and TST fluxes of ozone.

In our study, we find maxima in June (NH, 24.5 Tg month^{-1}) and January (SH, 20.4 Tg month^{-1}) and the minima are reached in January (NH, 15.2 Tg month^{-1}) and June (SH, 15.3 Tg month^{-1}). These values are calculated from the average daily fluxes in Fig. 16. Our maxima are roughly 50 % lower than the average of the Eulerian studies. This is to be expected since method inter-comparison and evaluation studies have shown that Eulerian models are too diffusive and are likely to overestimate STE fluxes (Cristofanelli et al., 2003; Meloen et al., 2003). Surprisingly, this is not the case for the minima where our values agree well with the previous studies.

The most notable difference between our results and the Eulerian studies is the relative timing of mass and ozone fluxes. While in Olsen et al. (2004) the STT ozone flux only lags the net mass flux by one month, our STT ozone flux peaks in summer in both hemispheres when the STT mass flux is lowest. Due to the small seasonal cycle of the TST mass flux, this is also true for the net mass flux (not shown). Thus our STT mass and ozone fluxes are nearly perfectly anticyclic, i.e. shifted by 6 months. The reason for this difference is that our seasonal cycle of ozone concentrations at the tropopause (peaking in summer, see bottom row in Fig. 16) has a much larger relative amplitude (seasonality) than the seasonal cycle of the STT mass flux and thus dominates the STT ozone flux. In Olsen et al. (2004), the seasonal cycles of mass and ozone fluxes have similar relative amplitudes and furthermore, ozone concentrations at the tropopause in the NH show a steep drop in summer.

If we assume, accepting the observational study by Thouret et al. (2006), that our ozone cycle at the tropopause peaks one month too late (see above) and we thus correct for this shift, the seasonal cycle of the STT ozone flux would also be shifted by one month, peak in May and its maximum value would increase by 5 % (not shown). This is also the month in which the net STE ozone flux (without the effects of deep convection) peaks in Tang et al. (2011).

ACPD
13, 11537–11595, 2013

The situation is very different for the subset of deep exchanges where the relative amplitude of the mass flux clearly dominates the ozone concentrations at the tropopause and the maximum deep STT ozone flux is reached in March in the NH and in September in the SH (Fig. 16). This is in very good agreement with Stohl et al. (2003) and other studies that found a late winter/early spring maximum of stratospheric influence on ozone concentrations at the surface in the NH. In order to roughly estimate the increase in ozone in the PBL due to deep STT, one can assume a certain PBL height, thus defining a "PBL volume", and calculate the change in ozone concentrations inside this volume due to the ozone flux into it. Using a PBL height of 1 km, a flux of $1\,kg\,km^{-2}\,yr^{-1}$ corresponds to an increase of the ozone concentration by 1.28 ppbv per day within the PBL. The daily ozone input from the stratosphere into the PBL estimated in this manner reaches several 100 ppbv per day at the peaks of the deep STT ozone flux. These values are unrealistically high because mixing, wet and dry deposition and chemical processes are changing the ozone concentrations in the free troposphere and the PBL. They however highlight the substantional potential of stratospheric intrusions to influence surface ozone in certain regions and seasons.

The large interannual variability of the deep STT ozone flux in the months between December and April in the NH (middle row on the left in Fig. 16) originates from exceptionally large values in the winters of 1997, 2000, 2002 and 2008, and the large variability of the STT ozone flux in September in the SH (top and middle row on the right in Fig. 16) is explained by exceptionally large peaks in the years of 1996, 1999, 2000 and 2001. Generally, the years from 1998 to 2002 are characterized by a very strong seasonal cycle and an ozone flux that is around 15 % larger than in the years before. To some extent, this can be confirmed by the MOZAIC measurements: Thouret et al. (2006) find 10–15 % higher ozone concentrations in the years 1998 and 1999. Their data however shows a decrease to only 5 % elevated levels in the years between 2001 and 2003 whereas our STT ozone flux stays roughly constant between 1999 and 2002 until it rapidly drops in 2002 and 2003. This further supports the assumption that there is a problem with the ozone field in ERA-Interim during this period.

ACPD
13, 11537–11595, 2013

5.4 Regional aspects

Western North America, stretching from the Rocky Mountains in the North to the western Sierra Madre in the South, is a region of high deep STT fluxes for both mass (Fig. 5) and ozone (Fig. 15). The maximum is reached in spring but fluxes are above average in all seasons. This result agrees well with recent studies that showed an important influence of STE in affecting ozone concentrations at the surface in this area (Lefohn et al., 2011, 2012; Lin et al., 2012). We also find that a lot of deep TST trajectories leave the PBL in this region, albeit slightly more to the east (Fig. 6). It seems that deep STT into the PBL occurs preferably on the upwind side of and right over the mountain ranges and the deep TST trajectories leave the PBL mostly on the downwind side.

The STT mass flux over Central Europe is comparatively intense in winter and spring and to a lesser degree also in fall, see Fig. 2. This is also true for the STT ozone flux across the 600 hPa surface (not shown) and supports the finding that the background ozone levels in the lower troposphere are affected by STT (Ordóñez et al., 2007). However, only in spring do the intrusions reach deep enough to influence the PBL, see Fig. 5. It is thus understandable that signatures of deep STT intrusions at the ground have mainly been observed at Alpine measurement sites in spring (Stohl et al., 2000; Trickl et al., 2010).

Both STT and TST mass fluxes in JJA have a distinct maximum over the Eastern Mediterranean and Anatolia, see Figs. 2 and 3. This is likely due to deep tropopause folds associated with the subtropical jet stream, enhancing turbulent mixing and STE (Sprenger et al., 2003; Traub and Lelieveld, 2003). In this region, there are elevated levels for deep STT in DJF and MAM (Fig. 5) indicating that deep stratospheric intrusions such as the one observed by Gerasopoulos et al. (2006) are not unusual.

Further to the east, the STT mass flux in JJA shows elevated values along the northern flank of the upper-level Asian monsoon anticyclone. Sprenger et al. (2003) found that this area is a hotspot for shallow and medium tropopause folds which explains the enhanced STT flux. Why this is not the case for the TST mass flux remains and open

ACPD
13, 11537–11595, 2013

question, and the interaction of the subtropical jet stream, the elevated topography and the upper-level anticyclone in this region will be subject to further investigations.

6 Conclusions

We have compiled a global climatology of STE using the state-of-the-art reanalysis dataset ERA-Interim over 33 yr from 1979 to 2011. The well-established Lagrangian methodology has been refined with a 3-D-labelling algorithm that distinguishes between the troposphere and the stratosphere (see Sect. 2.2) and a realistic representation of deep exchanges across the top of the PBL (see Sect. 2.3). In addition to the mass flux, assimilated ozone data has been used to calculate the ozone flux across the tropopause and into the PBL. The main results of this climatology are:

- The geographical distribution of STE shows strong zonal asymmetry and pronounced seasonal cycles, especially for the subset of deep exchange events. The storm tracks over the North Atlantic, North Pacific and the Southern Ocean as well as mountain chains in the subtropics are preferred regions of STE.
- There are clear hotspots of deep STT flux into the continental PBL. The Rocky Mountains and the other mountain ranges along the west coast of North America are affected all year around, with a clear peak in spring (MAM). There is also intense deep STT flux over the Tibetan Plateau during the whole year, with a peak in DJF. In the SH, the highest fluxes into the PBL are found over the Andes around 30° S. In the storm tracks, especially over the North Atlantic and the North Pacific in DJF and the Indian Ocean in JJA, deep STT events transport stratospheric air into the marine PBL.
- Air from the entrance of the North Atlantic and North Pacific storm tracks is rapidly transported into the stratosphere (deep TST) during all seasons but summer. Over the continents, the clear hotspots of deep TST are the Rocky Mountains and

ACPD
13, 11537–11595, 2013

mountain ranges nearby in spring (MAM) and the Tibetan Plateau in DJF and MAM. The deep TST maxima are preferably located on the downwind side of the orography, to the east of the deep STT maxima, which lie on the upwind side or directly over the high-altitude areas.

– STT dominates in the extratropics and TST in the tropics and polar regions. The mass flux by deep exchanges across the tropopause is limited to the extratropics and the flux into the PBL is shifted between roughly 15° (NH) and 30° (SH) towards the equator.

– The seasonal cycles of the mass fluxes vary strongly in amplitude and shape. STT is most intense during winter or early spring and reaches a minimum in summer in both hemispheres. For TST, the situation is more complex, as the deep TST mass flux is strongly out of phase with respect to the total TST mass flux. The seasonality of the total STE fluxes varies between $S = 3\,\%$ (STT SH) and $S = 12\,\%$ (STT NH). The seasonal cycles of deep STE are much more pronounced for both STT and TST in both hemispheres (seasonalities between $S = 28\,\%$ for deep TST and $S = 82\,\%$ for deep STT in the NH). The deep STT flux peaks in early spring in the NH and in winter in the SH. In both hemispheres, the minimum is reached in summer. The deep TST flux stays roughly constant between January and June in the NH, and drops sharply to a minimum in August. In the SH, the cycle is more smooth with a maximum in winter and a minimum in summer.

– The analysis of potential temperatures at the exchange location shows a broad and complex distribution in both hemispheres, further emphasizing that studies which focus on a few Θ-surfaces miss a substantial part of the exchange events. There is a clear connection between Θ and latitude such that the high-Θ events exclusively occur in the tropics. Deep STE occurs almost exclusively at Θ below 350 K.

ACPD
13, 11537–11595, 2013

– The time series over the 33 yr from 1979 to 2011 shows an increasing net downward flux and slightly decreasing gross fluxes. There are positive trends for both deep STT and deep TST mass fluxes but the downward flux increases twice as fast as the upward flux.

– The ozone flux across the tropopause is significantly influenced by the seasonal cycle and geographical distribution of ozone concentrations at the tropopause and thus prescribing a mean mixing ratio at the tropopause leads to erroneous results. There are pronounced peaks over the Andes (DJF), the Himalayas (MAM), the Tibetan Plateau (MAM, JJA), as well as central North America, Anatolia, the equator over the Indian ocean and much of East Asia in JJA.

– The ozone flux due to deep STT into the PBL is dominated by the seasonal and geographical variations of the deep STT mass flux. The global hotspots, where surface ozone concentrations are most likely influenced by STE are the mountain ranges along the west coast of North America, especially in MAM, and the Tibetan Plateau in all seasons except for SON. In the latter region, the very high orography, combined with a high mixing layer, enables quasi-horizontal transport into the PBL whereas for the former region, considerable vertical transport is necessary.

– The seasonal cycle of the STT ozone flux peaks in June, which contrasts the mass flux that is nearly at its minimum at that time. This shows that the STT ozone flux is dominated by the variation in prevailing ozone concentrations at the tropopause. The seasonal cycle of deep STT ozone flux, on the other hand, is clearly dominated by changes in the deep STT mass flux and peaks in early spring.

– The ozone field assimilated in ERA-Interim produces a reasonable seasonal cycle of ozone at the tropopause, yet there might be significant problems with the assimilation of data from satellite instruments during the period from 1995 to 2004. Our time series, which is especially affected by these problems, has thus

ACPD
13, 11537–11595, 2013

to be interpreted with care. Nevertheless, we obtain meaningful results for the geographical and seasonal distribution of the downward ozone flux across the tropopause and into the PBL.

- Where comparable, our results agree well with the findings of earlier Lagrangian studies and differ in some aspects from Eulerian studies using chemistry transport models in combination with the budget method.
- The mass and ozone fluxes across the tropopause, pressure surfaces and into as well as out of the PBL depend on the minimum residence time τ. This dependence follows a power-law ($c \cdot \tau^{\kappa}$) with remarkable accuracy ($R^2 > 0.995$). The fitted exponents κ vary from -0.87 for the TST mass flux to -0.44 for the STT ozone flux across the 700 hPa surface.
- Since the spatial and temporal resolution of our data is too coarse to capture convection, we are certainly underestimating the effect of (deep) convection on STE. For this reason, high-resolution STE diagnostics such as the one presented in Bourqui et al. (2012) and studies using mesoscale numerical weather prediction models (Gray, 2003; Lin et al., 2012) are of great importance.

Acknowledgements. We thank the ECMWF and MeteoSwiss for providing access to the meteorological data and Harald Sodemann for useful discussions.

References

Appenzeller, C., Holton, J., and Rosenlof, K.: Seasonal variation of mass transport across the tropopause, J. Geophys. Res., 101, 15071–15078, doi:10.1029/96JD00821, 1996. 11540, 11551, 11563

Berthet, G., Esler, J., and Haynes, P.: A Lagrangian perspective of the tropopause and the ventilation of the lowermost stratosphere, J. Geophys. Res., 112, D18102, doi:10.1029/2006JD008295, 2007. 11548

ACPD
13, 11537–11595, 2013

Bourqui, M.: Analysis and Quantification of STE: a Novel Approach, Ph.D. thesis, ETH Zurich, Switzerland, 2001. 11559

Bourqui, M. S.: Stratosphere-troposphere exchange from the Lagrangian perspective: a case study and method sensitivities, Atmos. Chem. Phys., 6, 2651–2670, doi:10.5194/acp-6-2651-2006, 2006. 11540, 11559

Bourqui, M. and Trepanier, P.: Descent of deep stratospheric intrusions during the IONS August 2006 campaign, J. Geophys. Res., 115, D18301, doi:10.1029/2009JD013183, 2010. 11539

Bourqui, M. S., Yamamoto, A., Tarasick, D., Moran, M. D., Beaudoin, L.-P., Beres, I., Davies, J., Elford, A., Hocking, W., Osman, M., and Wilkinson, R.: A new global real-time Lagrangian diagnostic system for stratosphere-troposphere exchange: evaluation during a balloon sonde campaign in eastern Canada, Atmos. Chem. Phys., 12, 2661–2679, doi:10.5194/acp-12-2661-2012, 2012. 11570

Chen, B., Xu, X. D., Yang, S., and Zhao, T. L.: Climatological perspectives of air transport from atmospheric boundary layer to tropopause layer over Asian monsoon regions during boreal summer inferred from Lagrangian approach, Atmos. Chem. Phys., 12, 5827–5839, doi:10.5194/acp-12-5827-2012, 2012. 11548

Collins, W., Derwent, R., Garnier, B., Johnson, C., Sanderson, M., and Stevenson, D.: Effect of stratosphere-troposphere exchange on the future tropospheric ozone trend, J. Geophys. Res., 108, 8528, doi:10.1029/2002JD002617, 2003. 11539

Cooper, O., Stohl, A., Hübler, G., Hsie, E., Parrish, D., Tuck, A., Kiladis, G., Oltmans, S., Johnson, B., Shapiro, M., Moody, J. L., and Lefohn, A. S.: Direct transport of midlatitude stratospheric ozone into the lower troposphere and marine boundary layer of the tropical Pacific Ocean, J. Geophys. Res., 110, D23310, doi:10.1029/2005JD005783, 2005. 11539, 11546

Cristofanelli, P., Bonasoni, P., Collins, W., Feichter, J., Forster, C., James, P., Kentarchos, A., Kubik, P., Land, C., Meloen, J., Roelofs, G. J., Siegmund, P., Sprenger, M., Schnabel, C., Stohl, A., Tobler, L., Tositti, L., Trickl, T., and Zanis, P.: Stratosphere-to-troposphere transport: a model and method evaluation, J. Geophys. Res., 108, 8525, doi:10.1029/2002JD002600, 2003. 11564

Cristofanelli, P., Bracci, A., Sprenger, M., Marinoni, A., Bonafè, U., Calzolari, F., Duchi, R., Laj, P., Pichon, J.M., Roccato, F., Venzac, H., Vuillermoz, E., and Bonasoni, P.: Tropospheric ozone variations at the Nepal Climate Observatory-Pyramid (Himalayas, 5079 m a.s.l.) and influence of deep stratospheric intrusion events, Atmos. Chem. Phys., 10, 6537–6549, doi:10.5194/acp-10-6537-2010, 2010. 11539, 11556

ACPD
13, 11537–11595, 2013

Danielsen, E.: Stratospheric-tropospheric exchange based on radioactivity, ozone and potential vorticity, J. Atmos. Sci., 25, 502–518, 1968. 11539

Davies, T. D. and Schuepbach, E.: Episodes of high ozone concentrations at the earth's surface resulting from transport down from the upper troposphere/lower stratosphere: a review and case studies, Atmos. Environ., 28, 53–68, doi:10.1016/1352-2310(94)90022-1, 1994. 11539

Dee, D. P., Uppala, S. M., Simmons, A. J., Berrisford, P., Poli, P., Kobayashi, S.,Andrae, U., Balmaseda, M. A., Balsamo, G., Bauer, P., Bechtold, P., Beljaars, A. C. M., van de Berg, L., Bidlot, J., Bormann, N., Delsol, C., Dragani, R., Fuentes, M., Geer, A. J., Haimberger, L., Healy, S. B., Hersbach, H., Holm, E. V., Isaksen, L., Kallberg, P., Köhler, M., Matricardi, M., McNally, A. P., Monge-Sanz, B. M., Morcette, J.- J., Park, B.- K., Peubey, C., de Rosnay, P., Tavolato, C., Thepaut, J.-N., and Vitart, F.: The ERA-Interim reanalysis: configuration and performance of the data assimilation system, Q. J. Roy. Meteor. Soc., 137, 553–597, doi:10.1002/qj.828, 2011. 11541, 11543, 11559, 11561

Dragani, R.: On the quality of the ERA-Interim ozone reanalyses: comparisons with satellite data, Q. J. Roy. Meteor. Soc., 137, 1312–1326, doi:10.1002/qj.821, 2011. 11555, 11560

Ertel, H.: Ein neuer hydrodynamischer Wirbelsatz, Meteorol. Z., 59, 271–281, 1942. 11541

Forster, P., Ramaswamy, V., Artaxo, P., Berntsen, T., Betts, R., Fahey, D., Haywood, J., Lean, J., Lowe, D., Myhre, J., Nganga, R., Prinn, G., Raga, M., Schulz, R., and van Dorland, R.: Changes in atmospheric constituents and in radiative forcing, Climatic Change, 20, Cambridge University Press, Cambridge, UK, 2007. 11539

Fueglistaler, S., Wernli, H., and Peter, T.: Tropical troposphere-to-stratosphere transport inferred from trajectory calculations, J. Geophys. Res., 109, D03108, doi:10.1029/2003JD004069, 2004. 11545

Gauss, M., Myhre, G., Pitari, G., Prather, M. J., Isaksen, I. S. A., Berntsen, T. K., Brasseur, G. P., Dentener, F. J., Derwent, R. G., Hauglustaine, D. A., Horowitz, L. W., Jacob, D. J., Johnson, M., Law, S., Mickley, L. J., Müller, J.- F., Plantevin, P.- H., Pyle, J. A., Rogers, H. L., Stevenson, D. S., Sundet, J. K., van Weele, M., and Wild, O.: Radiative forcing in the 21st century due to ozone changes in the troposphere and the lower stratosphere, J. Geophys. Res., 108, 4292, doi:10.1029/2002JD002624, 2003. 11539

Gerasopoulos, E., Zanis, P., Papastefanou, C., Zerefos, C., Ioannidou, A., and Wernli, H.: A complex case study of down to the surface intrusions of persistent stratospheric air over the Eastern Mediterranean, Atmos. Environ., 40, 4113–4125, doi:10.1016/j.atmosenv.2006.03.022, 2006. 11566

ACPD
13, 11537–11595, 2013

Gettelman, A. and Sobel, A.: Direct diagnoses of stratosphere-troposphere exchange, J. Atmos. Sci., 57, 3–16, 2000. 11540
Gettelman, A., Kinnison, D., Dunkerton, T., and Brasseur, G.: Impact of monsoon circulations on the upper troposphere and lower stratosphere, J. Geophys. Res., 109, D22101, doi:10.1029/2004JD004878, 2004. 11545, 11563
Gray, S.: A case study of stratosphere to troposphere transport: the role of convective transport and the sensitivity to model resolution, J. Geophys. Res., 108, 4590, doi:10.1029/2002JD003317, 2003. 11570
Hall, T. and Holzer, M.: Advective-diffusive mass flux and implications for stratosphere-troposphere exchange, Geophys. Res. Lett., 30, 1222, doi:10.1029/2002GL016419, 2003. 11558, 11559, 11595
Hegglin, M. and Shepherd, T.: Large climate-induced changes in ultraviolet index and stratosphere-to-troposphere ozone flux, Nat. Geosci., 2, 687–691, doi:10.1038/NGEO604, 2009. 11539, 11563
Holton, J., Haynes, P., McIntyre, M., Douglas, A., Rood, R., and Pfister, L.: Stratosphere-troposphere exchange, Rev. Geophys., 33, 403–440, 1995. 11540, 11541
Hoskins, B., McIntyre, M., and Robertson, A.: On the use and significance of isentropic potential vorticity maps, Q. J. Roy. Meteor. Soc., 111, 877–946, 1985. 11541
Hsu, J., Prather, M., and Wild, O.: Diagnosing the stratosphere-to-troposphere flux of ozone in a chemistry transport model, J. Geophys. Res., 110, D19305, doi:10.1029/2005JD006045, 2005. 11556, 11563
Jacobson, M.: Atmospheric Pollution: History, Science, and Regulation, Cambridge University Press, 2002. 11539
James, P., Stohl, A., Forster, C., Eckhardt, S., Seibert, P., and Frank, A.: A 15-year climatology of stratosphere-troposphere exchange with a Lagrangian particle dispersion model: 2. Mean climate and seasonal variability, J. Geophys. Res., 108, 8522, doi:10.1029/2002JD002639, 2003a. 11540
James, P., Stohl, A., Forster, C., Eckhardt, S., Seibert, P., and Frank, A.: A 15-year climatology of stratosphere-troposphere exchange with a Lagrangian particle dispersion model: 1. Methodology and validation, J. Geophys. Res., 108, 8519, doi:10.1029/2002JD002637, 2003b. 11551
Juckes, M.: The mass flux across the tropopause: Quasi-geostrophic theory, Q. J. Roy. Meteor. Soc., 123, 71–99, 1997. 11549

ACPD
13, 11537–11595, 2013

Junge, C. E.: Global ozone budget and exchange between stratosphere and troposphere, Tellus, 4, 363–377, 1962. 11539
Kentarchos, A. and Roelofs, G.: A model study of stratospheric ozone in the troposphere and its contribution to tropospheric OH formation, J. Geophys. Res., 108, 8517, doi:10.1029/2002JD002598, 2003. 11539
Knowlton, K., Rosenthal, J., Hogrefe, C., Lynn, B., Gaffin, S., Goldberg, R., Rosenzweig, C., Civerolo, K., Ku, J., and Kinney, P.: Assessing ozone-related health impacts under a changing climate, Environ. Health Persp., 112, 1557, doi:10.1289/ehp.7163, 2004. 11539
Kuang, S., Newchurch, M. J., Burris, J., Wang, L., Knupp, K., and Huang, G.: Stratosphere-to-troposphere transport revealed by ground-based lidar and ozonesonde at a midlatitude site, J. Geophys. Res., 117, 18305, doi:10.1029/2012JD017695, 2012. 11539
Lamarque, J. and Hess, P.: Cross-tropopause mass exchange and potential vorticity budget in a simulated tropopause folding, J. Atmos. Sci., 51, 2246–2246, 1994. 11540
Lefohn, A., Wernli, H., Shadwick, D., Limbach, S., Oltmans, S., and Shapiro, M.: The importance of stratospheric-tropospheric transport in affecting surface ozone concentrations in the western and northern tier of the United States, Atmos. Environ., 45, 4845–4857, doi:10.1016/j.atmosenv.2011.06.014, 2011. 11539, 11556, 11566
Lefohn, A., Wernli, H., Shadwick, D., Oltmans, S., and Shapiro, M.: Quantifying the importance of stratospheric-tropospheric transport on surface ozone concentrations at high- and low-elevation monitoring sites in the United States, Atmos. Environ., 62, 646–656, doi:10.1016/j.atmosenv.2012.09.004, 2012. 11539, 11556, 11566
Lin, M., Fiore, A. M., Cooper, O. R., Horowitz, L. W., Langford, A. O., Levy, H., Johnson, B. J., Naik, V., Oltmans, S. J., and Senff, C. J.: Springtime high surface ozone events over the western United States: quantifying the role of stratospheric intrusions, J. Geophys. Res., 117, D00V22, doi:10.1029/2012JD018151, 2012. 11566, 11570
Lippmann, M.: Health effects of ozone a critical review, Japca. J. Air Waste Ma., 39, 672–695, 1989. 11539
Marenco, A., Thouret, V., Nédélec, P., Smit, H., Helten, M., Kley, D., Karcher, F., Simon, P., Law, K., Pyle, J., Poschmann, G., von Wrede, R., Hume, C., and Cook, T.: Measurement of ozone and water vapor by Airbus in-service aircraft: the MOZAIC airborne program, an overview, J. Geophys. Res., 103, 25631–25642, 1998. 11563
Meloen, J., Siegmund, P., Van Velthoven, P., Kelder, H., Sprenger, M., Wernli, H., Kentarchos, A., Roelofs, G., Feichter, J., Land, C., Forster, C., James, P., Stohl, A., Collins, W.,

ACPD
13, 11537–11595, 2013

and Cristofanelli, P.: Stratosphere-troposphere exchange: a model and method intercomparison, J. Geophys. Res., 108, 8526, doi:10.1029/2002JD002274, 2003. 11564
Olsen, M. A., Schoeberl, M. R., and Douglass, A. R.: Stratosphere-troposphere exchange of mass and ozone, J. Geophys. Res., 109, D24114, doi:10.1029/2004JD005186, 2004. 11551, 11562, 11563, 11564
Orbe, C., Holzer, M., and Polvani, L. M.: Flux distributions as robust diagnostics of stratosphere-troposphere exchange, J. Geophys. Res., 117, D01302, doi:10.1029/2011JD016455, 2012. 11558, 11559
Ordóñez, C., Brunner, D., Staehelin, J., Hadjinicolaou, P., Pyle, J., Jonas, M., Wernli, H., and Prévôt, A.: Strong influence of lowermost stratospheric ozone on lower tropospheric background ozone changes over Europe, Geophys. Res. Lett., 34, L07805, doi:10.1029/2006GL029113, 2007. 11566
Roelofs, G. and Lelieveld, J.: Model study of the influence of cross-tropopause O_3 transports on tropospheric O_3 levels, Tellus B, 49, 38–55, 1997. 11539
Schmidt, T., Wickert, J., Beyerle, G., and Heise, S.: Global tropopause height trends estimated from GPS radio occulation data, Geophys. Res. Lett., 35, L11806, doi:10.1029/2008GL034012, 2008. 11554
Schoeberl, M.: Extratropical stratosphere-troposphere mass exchange, J. Geophys. Res., 109, D13303, doi:10.1029/2004JD004525, 2004. 11551
Seidel, D. and Randel, W.: Variability and trends in the global tropopause estimated from radiosonde data, J. Geophys. Res., 111, D21101, doi:10.1029/2006JD007363, 2006. 11554
Seo, K. and Bowman, K.: A climatology of isentropic cross-tropopause exchange, J. Geophys. Res., 106, 28159–28172, doi:10.1029/2000JD000295, 2001. 11540, 11553
Simmons, A., Uppala, S., Dee, D., and Kobayashi, S.: ERA-interim: new ECMWF reanalysis products from 1989 onwards, ECMWF Newsletter, 110, 26–35, 2006. 11541
Solomon, S., Qin, D., Manning, M., Alley, R. B., Berntsen, T., Bindoff, N.L., Chen, Z., Chidthaisong, A., Gregory, J. M., Hegerl, G. C., Heimann, M., Hewitson, B., Hoskins, B. J., Joos, F., Jouzel, J., Kattsov, V., Lohmann, U., Matsuno, T., Molina, M., Nicholls, N., Overpeck, J., Raga, G., Ramaswamy, V., Ren, J., Rusticucci, M., Somerville, R., Stocker, T. F., Stouffer, R. J., Whetton, P., Wood, R. A., and Wratt, D.: Climate Change 2007: the Physical Science Basis: Contribution of Working Group I to the Fourth Assessment Report of the Intergovernmental Panel on Climate Change, Cambridge University Press, 2007. 11555

ACPD
13, 11537–11595, 2013

Sprenger, M. and Wernli, H.: A northern hemispheric climatology of cross-tropopause exchange for the ERA15 time period (1979–1993), J. Geophys. Res., 108, 8521, doi:10.1029/2002JD002636, 2003. 11540

Sprenger, M., Croci-Maspoli, M., and Wernli, H.: Tropopause folds and cross-tropopause exchange: A global investigation based upon ECMWF analyses for the time period March 2000 to February 2001, J. Geophys. Res., 108, 8518, doi:10.1029/2002JD002587, 2003. 11542, 11544, 11545, 11566, 11578

Steinbrecht, W., Claude, H., Köhler, U., and Hoinka, K.: Correlations between tropopause height and total ozone: implications for long-term changes, J. Geophys. Res., 103, 19183–19192, doi:10.1029/98JD01929, 1998. 11554

Stevenson, D. S., Dentener, F. J., Schultz, M. G., Ellingsen, K., van Noije, T. P. C., Wild, O., Zeng, G., Amann, M., Atherton, C. S., Bell, N., Bergmann, D. J., Bey, I., Butler, T., Cofala, J., Collins, W. J., Derwent, R. G., Doherty, R. M., Drevet, J., Eskes, H. J., Fiore, A. M., Gauss, M., Hauglustaine, D. A., Horowitz, L. W., Isaksen, I. S. A., Krol, M. C., Lamarque, J.-F., Lawrence, M. G., Montanaro, V., Müller, J.- F., Pitari, G., Prather, M. J., Pyle, J. A., Rast, S., Rodriguez, J. M., Sanderson, M. G., Savage, N. H., Shindell, D. T., Strahan, S. E., Sudo, K., and Szopa, S.: Multimodel ensemble simulations of present-day and near-future tropospheric ozone, J. Geophys. Res., 111, D08301, doi:10.1029/2005JD006338, 2006. 11539, 11555

Stohl, A., Spichtinger-Rakowsky, N., Bonasoni, P., Feldmann, H., Memmesheimer, M., Scheel, H., Trickl, T., Hübener, S., Ringer, W., and Mandl, M.: The influence of stratospheric intrusions on alpine ozone concentrations, Atmos. Environ., 34, 1323–1354, doi:10.1016/S1352-2310(99)00320-9, 2000. 11539, 11566

Stohl, A., Bonasoni, P., Cristofanelli, P., Collins, W., Feichter, J., Frank, A., Forster, C., Gerasopoulos, E., Gäggeler, H., James, P., Kentarchos, A. S., Kromp-Kolb, H., Krüger, B., Land, C., Meloen, J., Papayannis, A., Priller, A., Seibert, P., Sprenger, M., Roelofs, G. J., Scheel, H. E., Schnabel, C., Siegmund, P., Tobler, L., Trickl, T., Wernli, H., Wirth, V., Zanis, P., and Zerefos, C.: Stratosphere-troposphere exchange: a review, and what we have learned from STACCATO, J. Geophys. Res., 108, 8516, doi:10.1029/2002JD002490, 2003. 11540, 11565

Stohl, A., Forster, C., Frank, A., Seibert, P., and Wotawa, G.: Technical note: The Lagrangian particle dispersion model FLEXPART version 6.2, Atmos. Chem. Phys., 5, 2461–2474, doi:10.5194/acp-5-2461-2005, 2005. 11548

ACPD
13, 11537–11595, 2013

Tang, Q., Prather, M., and Hsu, J.: Stratosphere-troposphere exchange ozone flux related to deep convection, Geophys. Res. Lett., 38, L03806, doi:10.1029/2010GL046039, 2011. 11556, 11560, 11564

Thouret, V., Cammas, J.-P., Sauvage, B., Athier, G., Zbinden, R., Nédélec, P., Simon, P., and Karcher, F.: Tropopause referenced ozone climatology and inter-annual variability (1994–2003) from the MOZAIC programme, Atmos. Chem. Phys., 6, 1033–1051, doi:10.5194/acp-6-1033-2006, 2006. 11563, 11564, 11565

Traub, M. and Lelieveld, J.: Cross-tropopause transport over the eastern Mediterranean, J. Geophys. Res., 108, 4712, doi:10.1029/2003JD003754, 2003. 11566

Trickl, T., Feldmann, H., Kanter, H.-J., Scheel, H.-E., Sprenger, M., Stohl, A., and Wernli, H.: Forecasted deep stratospheric intrusions over Central Europe: case studies and climatologies, Atmos. Chem. Phys., 10, 499–524, doi:10.5194/acp-10-499-2010, 2010. 11539, 11566

Vingarzan, R.: A review of surface ozone background levels and trends, Atmos. Environ., 38, 3431–3442, doi:10.1016/j.atmosenv.2004.03.030, 2004. 11539

Wei, M.: A new formulation of the exchange of mass and trace constituents between the stratosphere and troposphere, J. Atmos. Sci., 44, 3079–3086, 1987. 11540

Wernli, H. and Bourqui, M.: A Lagrangian 1-year climatology of (deep) cross-tropopause exchange in the extratropical Northern Hemisphere, J. Geophys. Res., 107, 4021, doi:10.1029/2001JD000812, 2002. 11539

Wernli, H. and Davies, H. C.: A Lagrangian-based analysis of extratropical cyclones. I: the method and some applications, Q. J. Roy. Meteor. Soc., 123, 467–489, 1997. 11541

Wild, O.: Modelling the global tropospheric ozone budget: exploring the variability in current models, Atmos. Chem. Phys., 7, 2643–2660, doi:10.5194/acp-7-2643-2007, 2007. 11539

Wirth, V. and Egger, J.: Diagnosing extratropical synoptic-scale stratosphere-troposphere exchange: a case study, Q. J. Roy. Meteor. Soc., 125, 635–655, doi:10.1002/qj.49712555413, 1999. 11540

Yang, K., Koike, T., Fujii, H., Tamura, T., Xu, X., Bian, L., and Zhou, M.: The daytime evolution of the atmospheric boundary layer and convection over the Tibetan Plateau: observations and simulations, J. Meteorol. Soc. Jpn., 82, 1777–1792, doi:10.2151/jmsj.82.1777, 2004. 11546, 11560

Zeng, G. and Pyle, J. A.: Changes in tropospheric ozone between 2000 and 2100 modeled in a chemistry-climate model, Geophys. Res. Lett., 30, 1392, doi:10.1029/2002GL016708, 2003. 11539

ACPD
13, 11537–11595, 2013

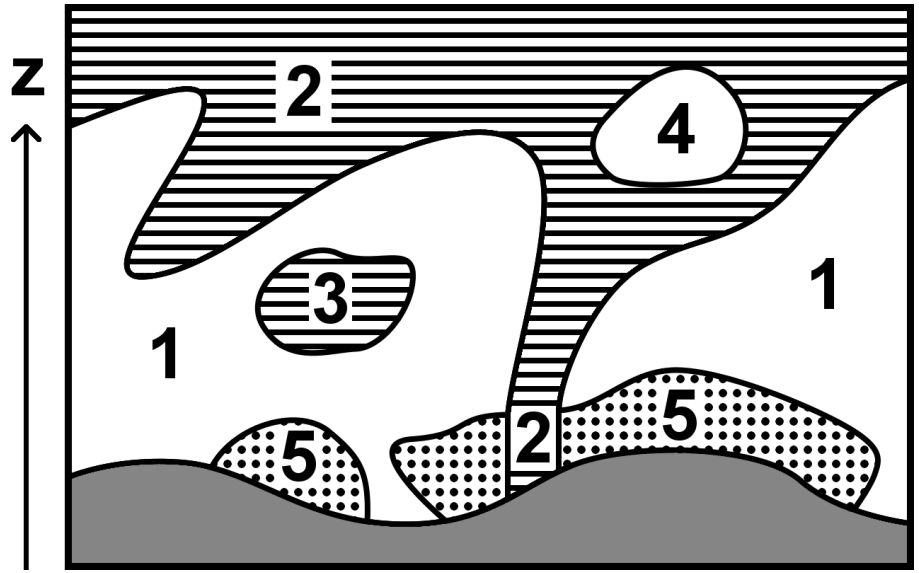

Fig. 1. The 3-D-labelling algorithm assigns labels from 1 to 5 to every grid point based on PV and Θ and the "connectivity" to the top of the ERA-Interim dataset or the surface (see Sprenger et al., 2003). The labels used are: 1 = troposphere, 2 = stratosphere, 3 = stratospheric cut-off in the troposphere or other cyclonic PV anomaly not connected to the stratosphere, 4 = tropospheric cut-off in the stratosphere and 5 = surface-bound PV anomalies. In the special cases where label 2 merges with label 5, the label 2 is attributed to grid points in the vertical column below the area of contact. Only if the contact occurs in the upper half of the troposphere (in this vertical column), the label 2 can propagate horizontally.

ACPD
13, 11537–11595, 2013

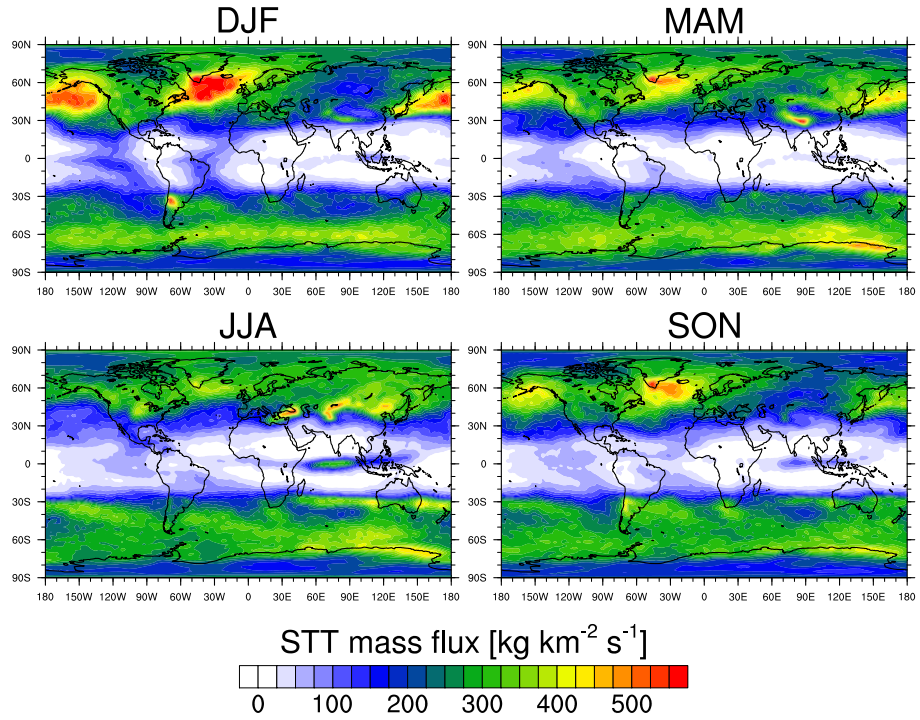

Fig. 2. Seasonally averaged STT mass flux for 1979–2011 (DJF = December, January, February, MAM = March, April, May, JJA = June, July, August, SON = September, October, November).

ACPD
13, 11537–11595, 2013

A global climatology of stratosphere-troposphere exchange

B. Skerlak

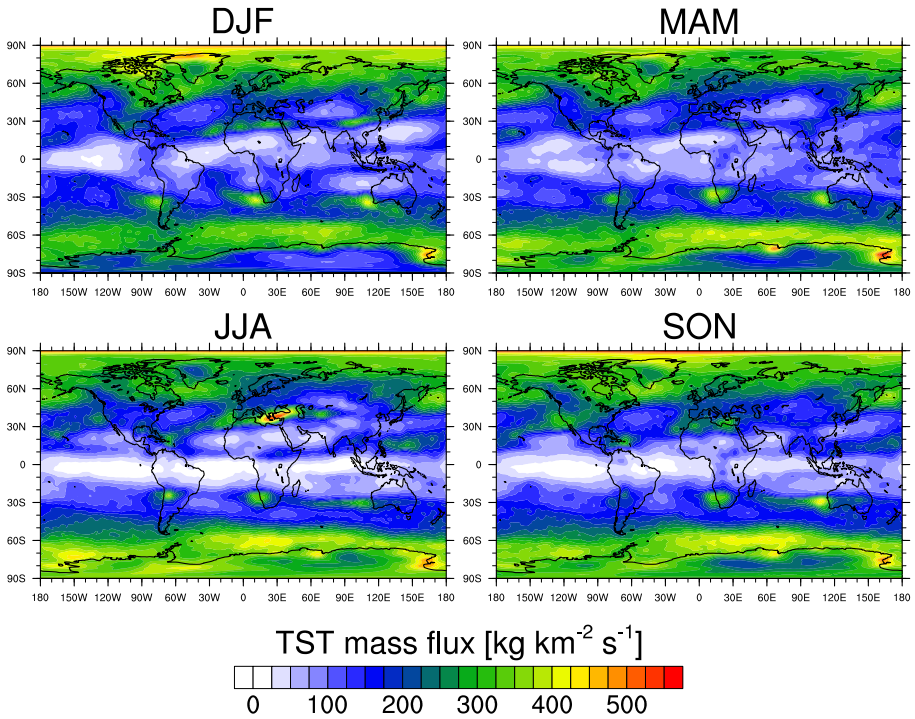

Fig. 3. Seasonally averaged TST mass flux for 1979–2011.

ACPD
13, 11537–11595, 2013

A global climatology of stratosphere-troposphere exchange

B. Skerlak

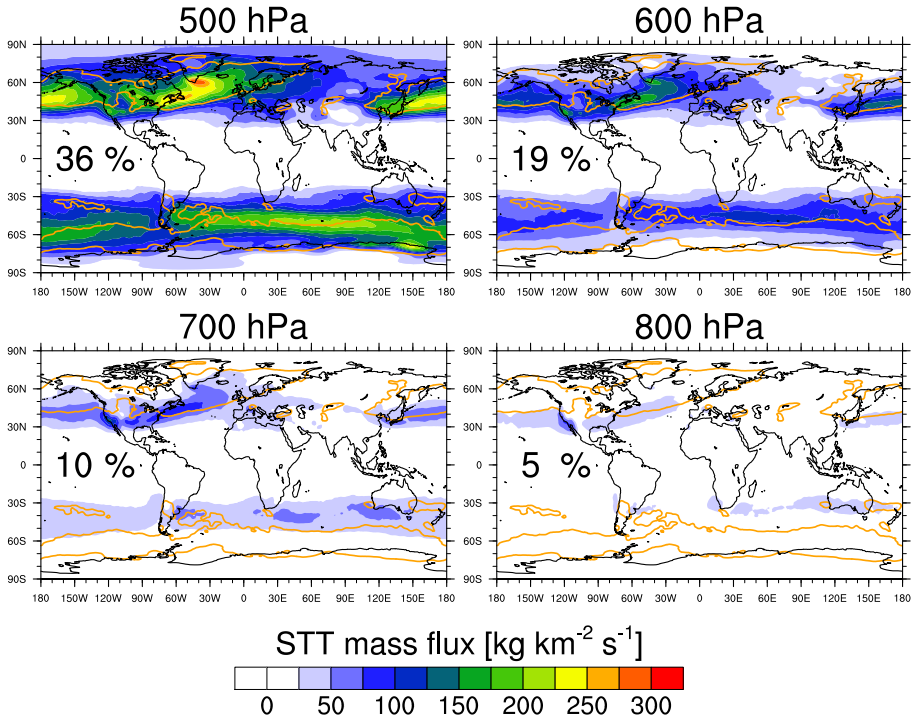

Fig. 4. STT mass flux through the 500, 600, 700 and 800 hPa pressure surfaces of all STT events averaged over the period from 1979 to 2011. The orange contours indicate areas where the STT mass flux across the tropopause is greater than 300 kg km^{-2} s^{-1}. The percentage values indicated in the panels are calculated with respect to the global STT mass flux across the tropopause.

ACPD
13, 11537–11595, 2013

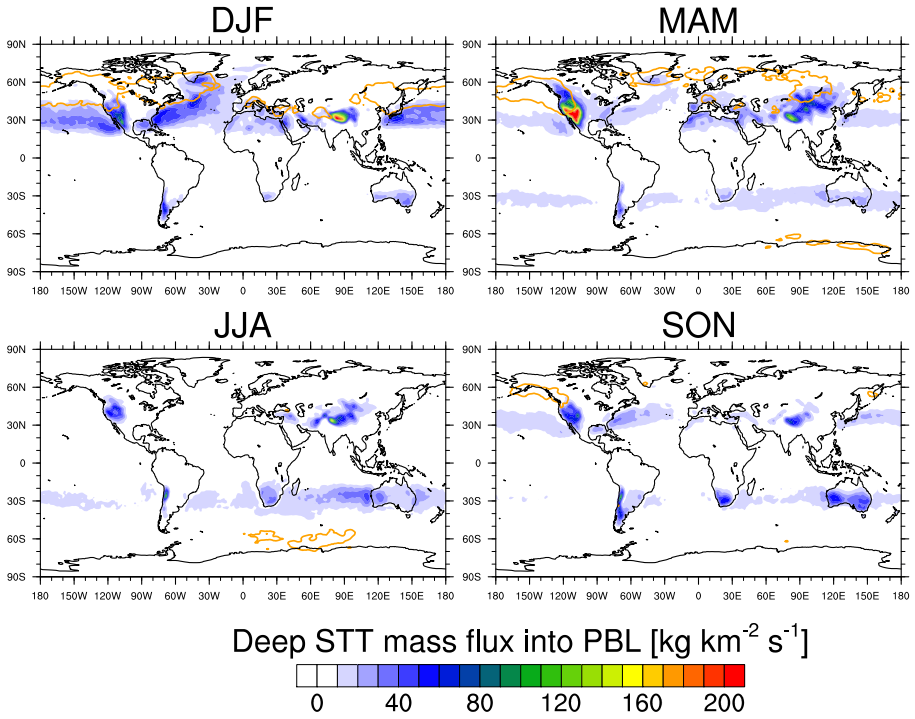

Fig. 5. Seasonally averaged mass flux into the PBL by deep STT events for 1979–2011. The orange contours indicate areas where the mass flux across the tropopause due to deep STT is higher than 25 kg km^{-2} s^{-1}.

ACPD
13, 11537–11595, 2013

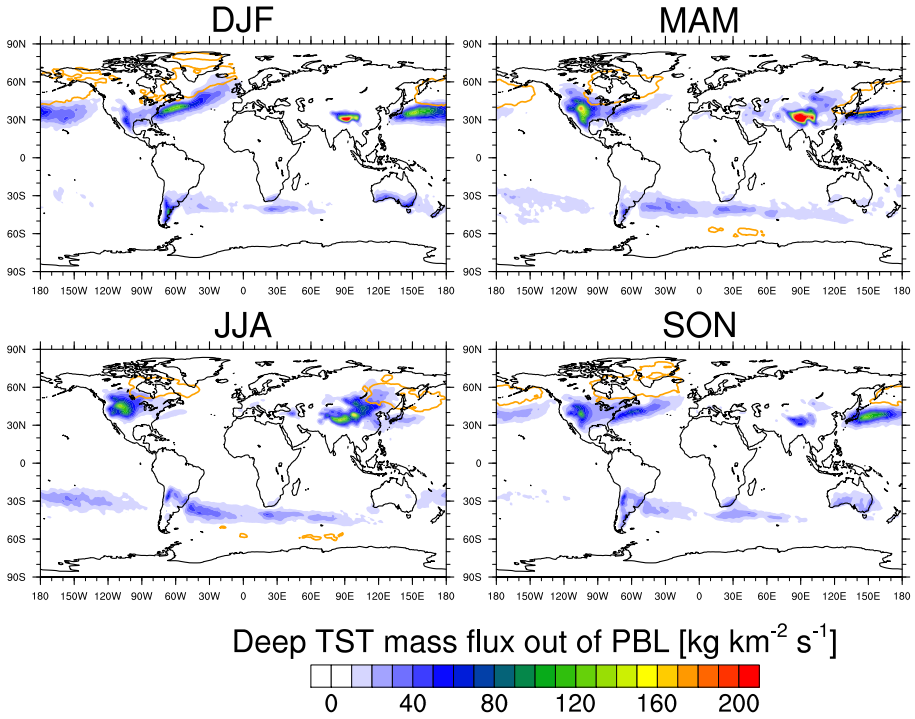

Fig. 6. Seasonally averaged mass flux out of the PBL by deep TST events for 1979–2011. The orange contours indicate areas where the mass flux across the tropopause due to deep TST is higher than 25 kg km^{-2} s^{-1}.

ACPD
13, 11537–11595, 2013

A global climatology of stratosphere-troposphere exchange

B. Skerlak

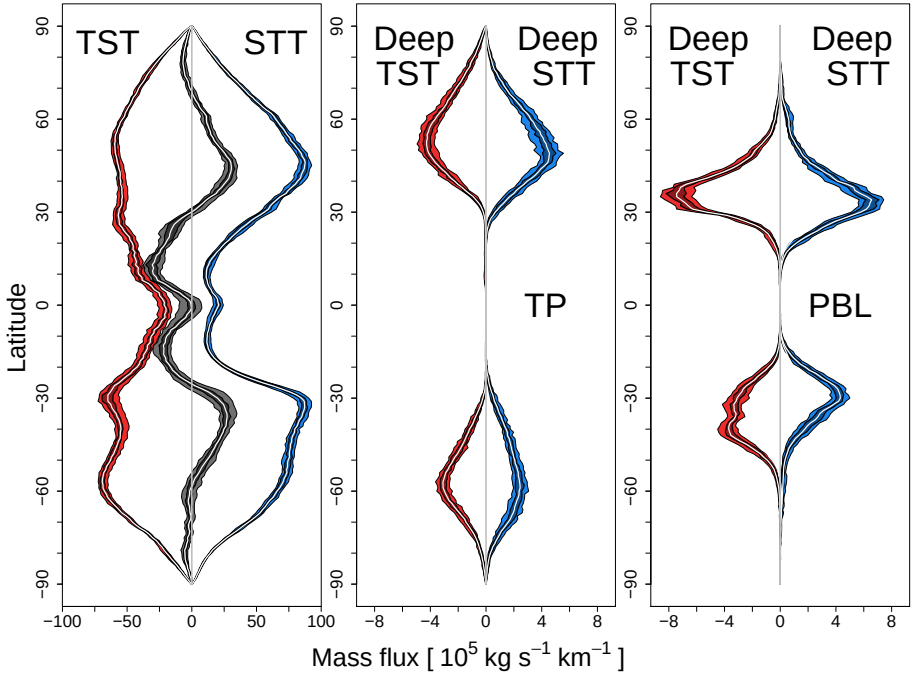

Fig. 7. Meridional distribution of zonally integrated cross-tropopause mass fluxes averaged from 1979 to 2011. The STT, TST and net(STT-TST) fluxes are shown on the left and the STT and TST fluxes of deep exchanges only are shown in the middle. The right panel shows the fluxes of deep exchanges into (STT) and out of (TST) the PBL. STT fluxes are shown positive (blue) and TST fluxes negative (red). The gray curve in the left panel shows the net flux. The shading shows the 5 % and 95 % (light) and the 25 % and 75 % (dark) percentiles of the individual annual values, and the white line is the mean value of the 33 yr investigated.

ACPD
13, 11537–11595, 2013

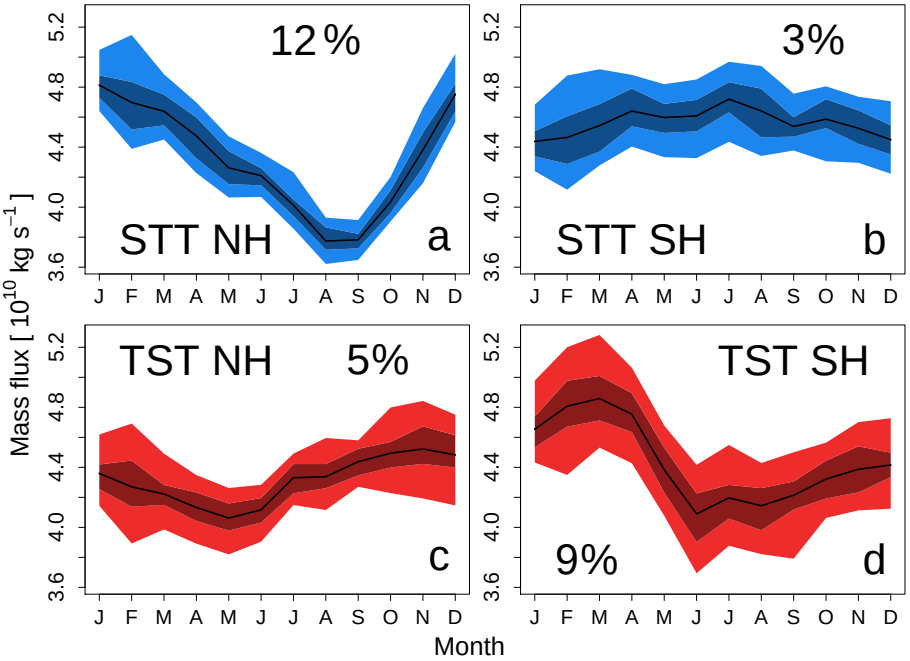

Fig. 8. Seasonal cycle of hemispherically integrated STT (blue, top) and TST (red, bottom) mass fluxes by all exchange events in the NH (left) and SH (right) averaged from 1979 to 2011. The shading shows the 5 % and 95 % (light) and the 25 % and 75 % (dark) percentiles of the annual values, and the solid black line is the mean value of the 33 yr. The seasonality is quantified by $S = \frac{\max - \min}{\max + \min}$ where max and min denote the maximum and minimum value of the mean cycle.

ACPD
13, 11537–11595, 2013

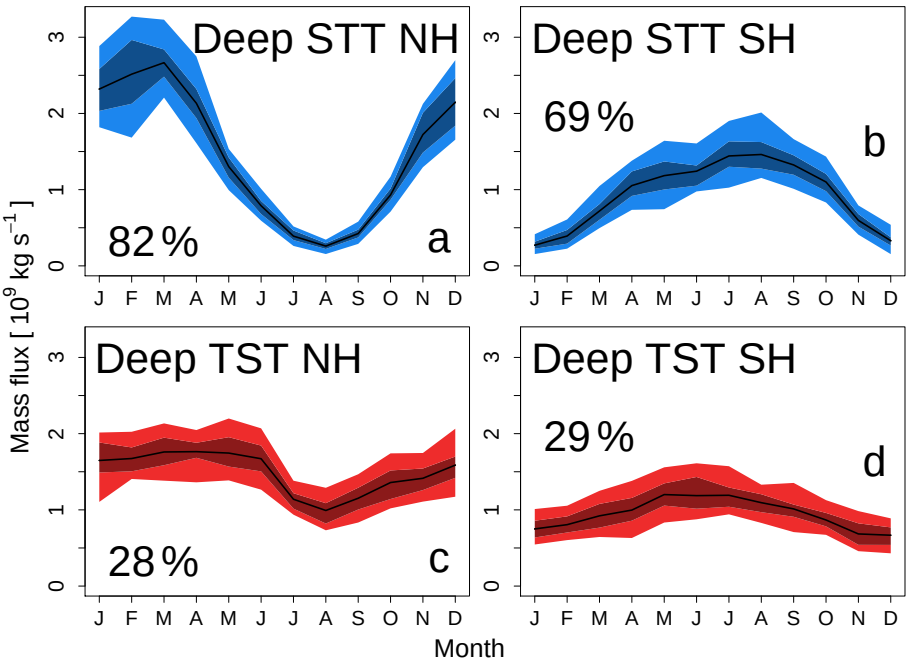

Fig. 9. Seasonal cycle of hemispherically integrated STT (blue, top) and TST (red, bottom) mass fluxes by deep exchange events in the NH (left) and SH (right) averaged from 1979 to 2011. The shading shows the 5 % and 95 % (light) and the 25 % and 75 % (dark) percentiles of the annual values, and the solid black line is the mean value of the 33 yr. The seasonality is quantified as in Fig. 8.

ACPD
13, 11537–11595, 2013

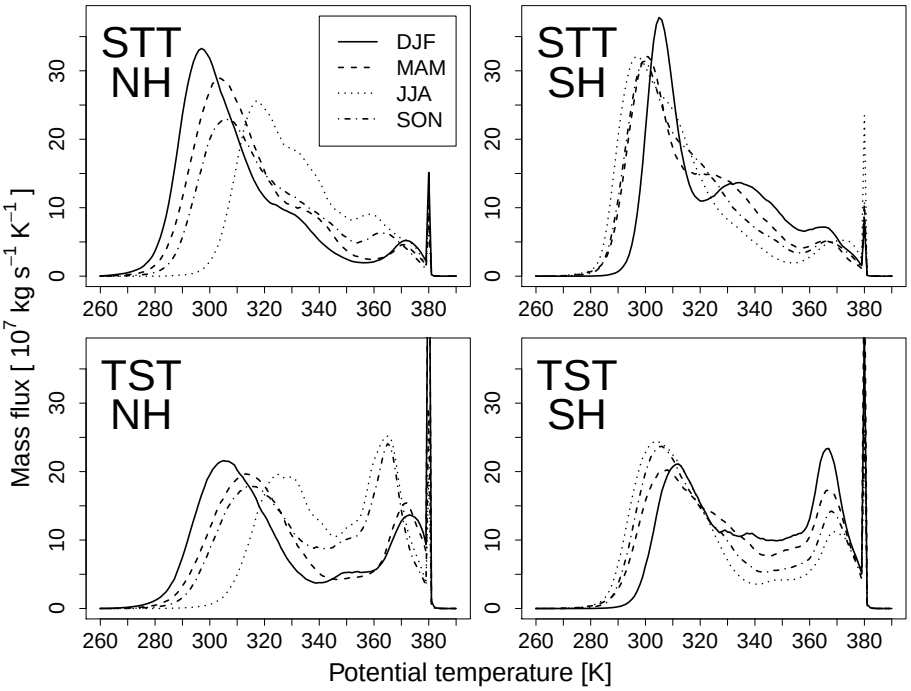

Fig. 10. Potential temperature distribution for STT (top) and TST (bottom) in the NH (left) and SH (right) averaged from 1979 to 2011. The seasons are indicated by different line patterns as listed in the legend.

ACPD
13, 11537–11595, 2013

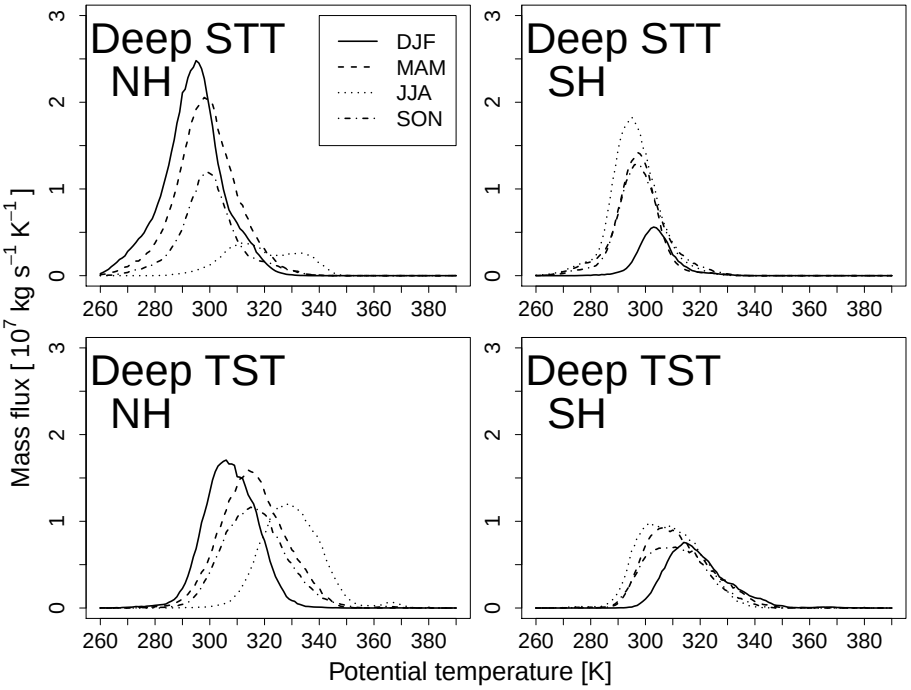

Fig. 11. Potential temperature distribution for deep STT (top) and deep TST (bottom) in the NH (left) and SH (right) averaged from 1979 to 2011. The seasons are indicated by different line patterns as listed in the legend.

ACPD
13, 11537–11595, 2013

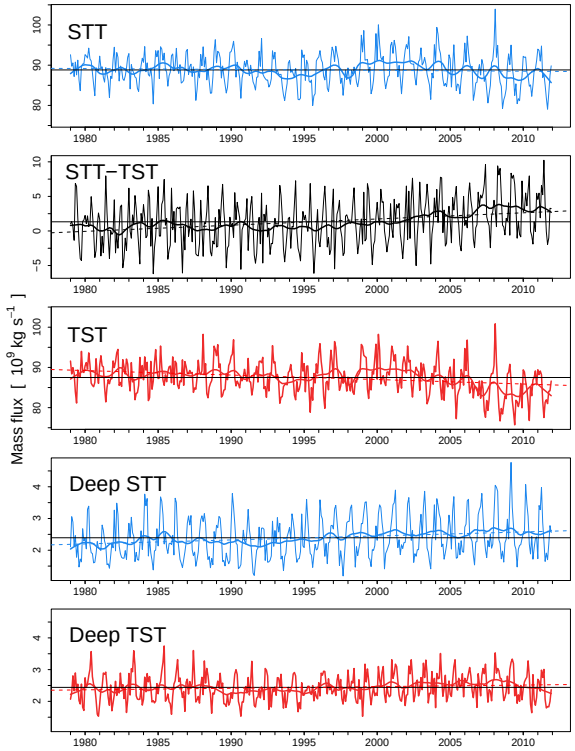

Fig. 12. Time series of globally integrated STT, TST, net (STT–TST), deep STT and deep TST mass fluxes from 1979 to 2011. The bold line is a 12 month moving average, the thin horizontal line is the mean value and the thin sloping line is the fit from a linear regression over the whole period. All trends except for the STT mass flux are significant on a 5 % level.

ACPD
13, 11537–11595, 2013

A global climatology of stratosphere-troposphere exchange

B. Skerlak

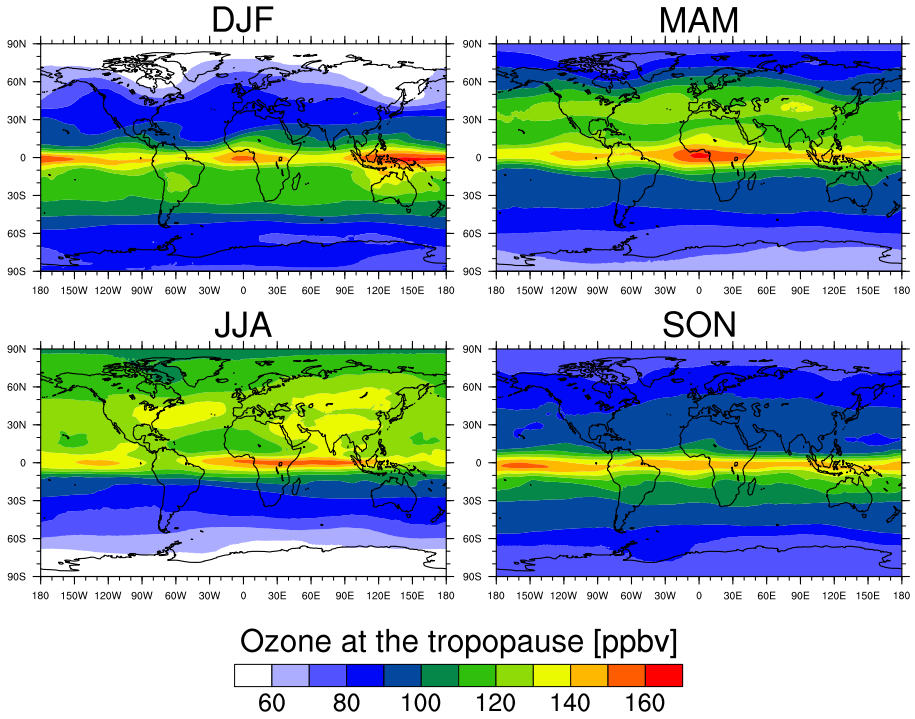

Fig. 13. Seasonally averaged ozone mixing ratios per volume (ppbv) at the 2 pvu/380 K tropopause for 1979–2011.

ACPD
13, 11537–11595, 2013

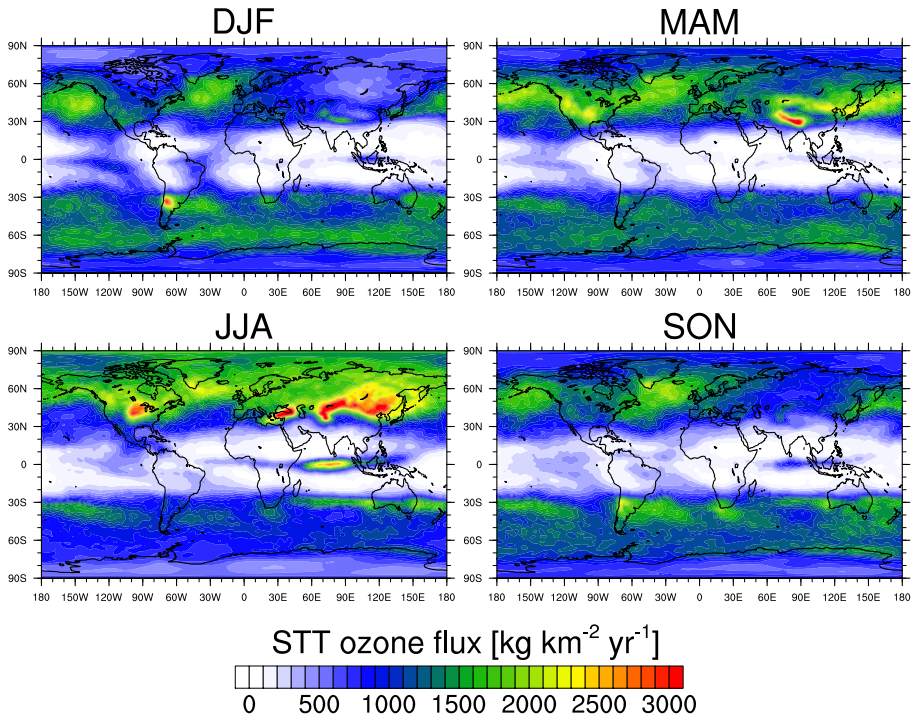

Fig. 14. Seasonally averaged STT ozone flux across the tropopause for 1979–2011.

ACPD
13, 11537–11595, 2013

A global climatology of stratosphere-troposphere exchange

B. Skerlak

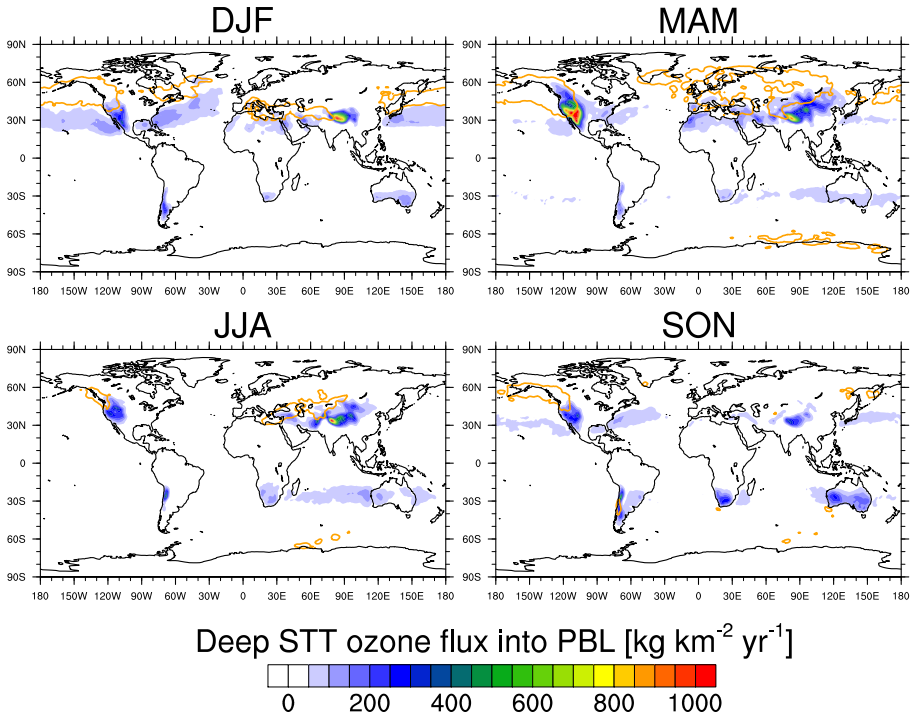

Fig. 15. Seasonally averaged deep STT ozone flux into the PBL for 1979–2011. The orange contours indicate areas where the ozone flux across the tropopause due to deep STT is higher than 80 kg km^{-2} yr^{-1}. For this calculation, the ozone concentration is kept constant along the trajectories after crossing the tropopause.

ACPD
13, 11537–11595, 2013

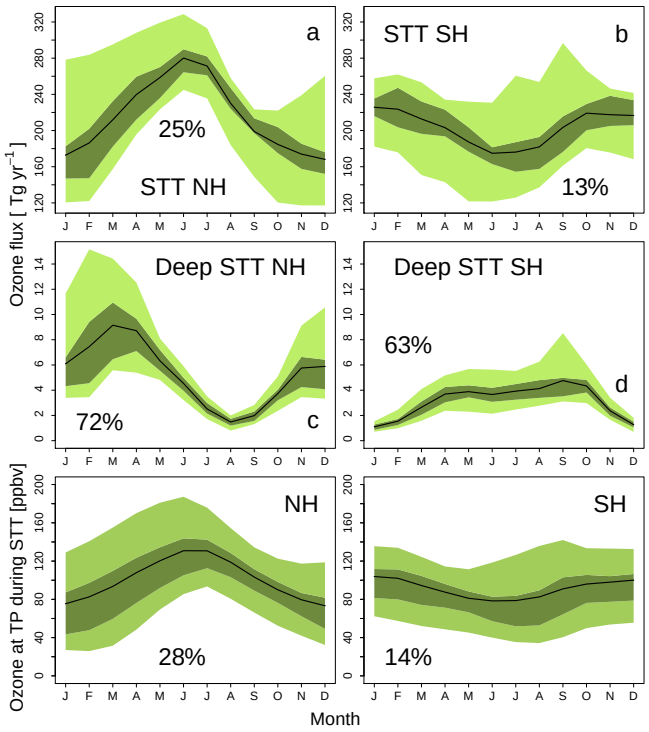

Fig. 16. Seasonal cycles of total STT ozone flux (top) and by deep exchange events only (middle) in the NH (left) and SH (right) averaged from 1979 to 2011. The bottom row shows the mean ozone concentration at the tropopause during STT events (weighted by the STT mass flux). The shaded areas show 5 % and 95 % (light) as well as 25 % and 75 % (dark) quantiles of the annual values. The black lines show the mean values of the 33 yr. The seasonality is quantified by $S = \frac{\max - \min}{\max + \min}$ where max and min denote the maximum and minimum value of the mean cycle.

ACPD
13, 11537–11595, 2013

A global climatology of stratosphere-troposphere exchange

B. Skerlak

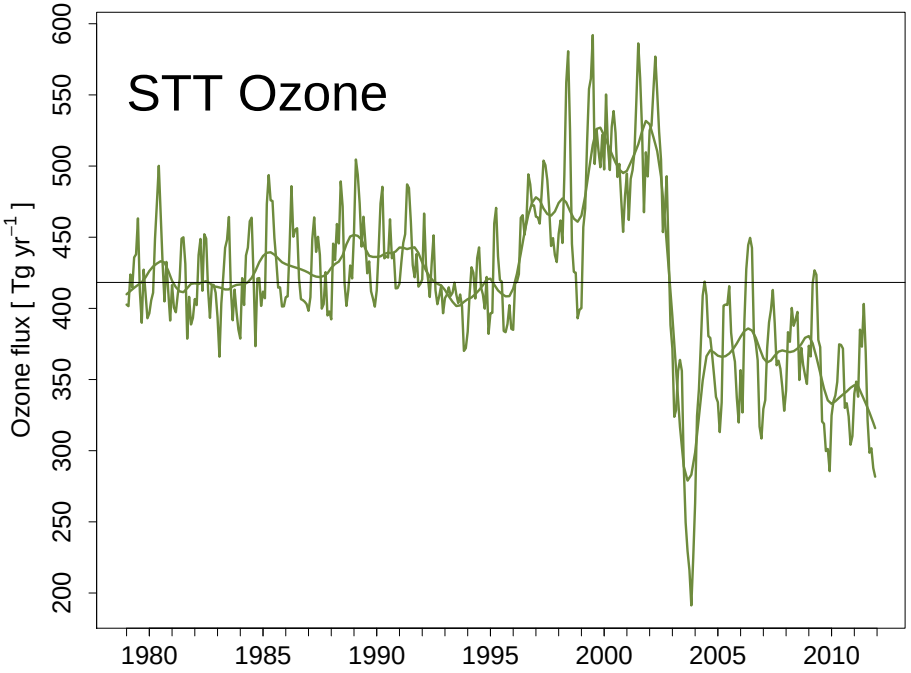

Fig. 17. Time series of the globally integrated STT ozone flux from 1979 to 2011. The bold line shows a 12 month moving average and the mean value of the whole time series is indicated with a horizontal line.

ACPD
13, 11537–11595, 2013

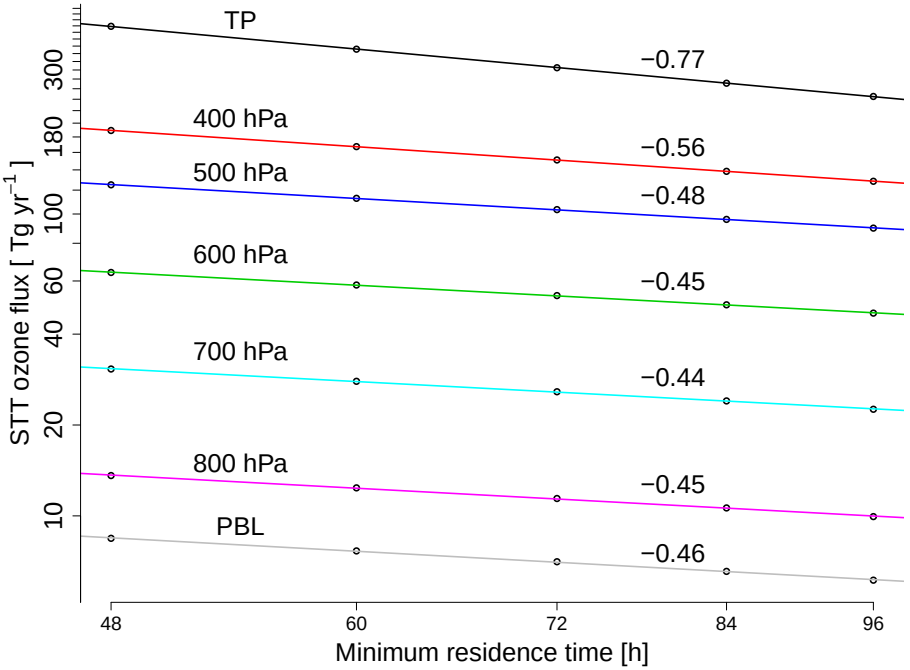

Fig. 18. Total STT ozone flux across the tropopause, pressure surfaces from 400 hPa to 800 hPa and into the PBL averaged for 1979–2011 and plotted on a double-logarithmic scale. The flux decreases with increasing minimum residence time threshold τ as a power law, i.e. the flux is proportional to τ^{κ}. The fitted exponents κ ($R^2 > 0.995$ for all fits) are listed adjacent to the corresponding curves. Theory suggests a value of −0.5 in the limit of very small τ (Hall and Holzer, 2003).

ACPD
13, 11537–11595, 2013